Continental Shelf Research 148 (2017) 159–177

Contents lists available at ScienceDirect

Continental Shelf Research

journal homepage: www.elsevier.com/locate/csr

Observations of the sub-inertial, near-surface East India Coastal Current

S. Mukhopadhyay[a,b], D. Shankar[a,b,*], S.G. Aparna[a], A. Mukherjee[c]

[a] CSIR-National Institute of Oceanography, Dona Paula, Goa 403004, India
[b] Academy of Scientific and Innovative Research, CSIR-NIO, Goa, India
[c] ESSO-Indian National Centre for Ocean Information Services, Hyderabad, India

ARTICLE INFO

Keywords:
Intraseasonal variability
Western boundary currents
HF radar
CODAR
ADCP
Bay of Bengal
Indian Ocean

ABSTRACT

We present surface current measurements made using two pairs of HF (high-frequency) radars deployed on the east coast of India. The radar data, used in conjunction with data from acoustic Doppler current profiler (ADCP) measurements on the shelf and slope off the Indian east coast, confirm that the East India Coastal Current (EICC) flows poleward as a deep current during February–March. During the summer monsoon, when the EICC flows poleward, and October–December, when the EICC flows equatorward, the current is shallow (<40 m deep), except towards the northern end of the coast. Data from Argo floats confirm a shallow mixed layer that leads to a strong vertical shear off southeast India during October–December. A consequence of the strong stratification is that the upward propagation of phase evident in the ADCP data does not always extend to the surface. Even within the seasons, however, the poleward and equatorward flows show variability at periods of the order of 20–45 days, implying that the EICC direction is the same over the top ~100 m for short durations. The high spatial resolution of the HF radar data brings out features at scales shorter than those resolved by the altimeter and the high temporal resolution captures short bursts that are not captured in satellite-derived estimates of surface currents. The radar data show that the EICC, which is a boundary current, leaves a strong imprint on the current at the coast. Since the EICC is known to be affected significantly by remote forcing, this correlation between the boundary and nearshore current implies the need to use large-domain models even for simulating the nearshore current. Comparison with a simulation by a state-of-the-art Ocean General Circulation Model, run at a resolution of 0.1° × 0.1°, shows that the model is able to simulate only the low-frequency variability.

1. Introduction

The East India Coastal Current (EICC) is the boundary current at the western margin of the Bay of Bengal (hereafter often called BoB or just bay), the eastern wing of the North Indian Ocean (NIO). The seasonal cycle of the EICC has been described using data from ship drifts (Cutler and Swallow, 1984; Mariano et al., 1995) and hydrography (Shetye et al., 1991, 1993, 1996); excellent summaries of these observations are available (Shetye and Gouveia, 1998; Schott and McCreary, 2001; Mukherjee et al., 2014) and we provide but some details here.

The ship-drift and hydrographic data show that the EICC flows poleward near the surface during February–September and equatorward during November–January (Shetye et al., 1991, 1993, 1996). Though the southwesterly summer-monsoon (June–September) winds along the east coast of India are much stronger than the winds during the transition period in March–April between the winter (November–February) and summer monsoons, the poleward EICC is much stronger during this period of weak winds. Model studies of the climatological seasonal cycle show that this discrepancy between the strength of the EICC and the local wind forcing is due to the significant impact of remote forcing, which includes the effect of Ekman pumping in the interior of the bay, the winds blowing along the eastern boundary of the bay, and the winds over the equatorial Indian Ocean (EIO; (McCreary et al., 1993, 1996; Shankar et al., 1996; Vinayachandran et al., 1996)). This interplay between the locally (winds blowing along the east coasts of India and Sri Lanka) and remotely forced components determines the magnitude and direction of the EICC at the surface and at sub-surface levels. For example, an undercurrent has been identified during the summer monsoon (Shetye et al., 1991) and model studies suggest that it is forced remotely (McCreary et al., 1996; Vinayachandran et al., 1996). The data also suggest that the upsloping of isopycnals is restricted to shallower depths during the summer monsoon (Shetye et al., 1991) than during March–April, when the poleward EICC extends much deeper (Shetye et al., 1993); the equatorward EICC during the winter monsoon is also shallow (Shetye et al., 1996).

* Corresponding author at: CSIR-National Institute of Oceanography, Dona Paula, Goa 403004, India.
E-mail address: shankar@nio.org (D. Shankar).

http://dx.doi.org/10.1016/j.csr.2017.08.020
Received 2 November 2016; Received in revised form 16 August 2017; Accepted 29 August 2017
Available online 08 September 2017
0278-4343/

Satellite altimeter data, which became available towards the end of 1992, allow the description to be extended beyond the seasonal climatology. The altimeter data confirm that the EICC forms the western-boundary current of a basin-scale seasonal gyre during March–April, but such a gyre is not evident during the summer monsoon (Eigenheer and Quadfasel, 2000; Shankar et al., 2002); this difference on the large scale had been suggested earlier on the basis of hydrographic data (Shetye et al., 1991, 1993) and satellite data of sea-surface temperature (Legeckis, 1987). Along-track altimeter data confirm the earlier ideas of the seasonal EICC and show that the cross-shore length scale varies from 60 to 150 km from north to south along the coast and that the interannual and intraseasonal EICC are comparable to the seasonal EICC (Durand et al., 2009). Unlike the seasonal EICC, however, the interannual and intraseasonal EICC are not coherent along the coast: they decorrelate along the coast. Eddy-like circulations, whose existence had been hinted at by Shetye et al. (1991), are seen in the altimeter data at both intraseasonal (Durand et al., 2009; Cheng et al., 2013) and interannual (Durand et al., 2009; Chen et al., 2012) periods in the regime of the EICC, which exhibits several meso-scale structures irrespective of the season (Kurien et al., 2010).

Prior to 2009, direct measurements of the EICC were few and were restricted to short durations; a summary of these measurements is given in Mukherjee et al. (2014), who present the data collected using ADCP (acoustic Doppler current profiler) moorings deployed on the continental slope off the Indian east coast under a programme on observing the boundary currents in the Indian Exclusive Economic Zone (EEZ). The ADCP data confirm the earlier findings regarding the seasonal reversal of the EICC, but show that the seasonal component is stronger than the intraseasonal component (Mukherjee et al., 2014), unlike for the West India Coastal Current (WICC), whose intraseasonal variability is comparable to or stronger than its seasonal cycle (Vialard et al., 2009; Amol et al., 2014). Striking in these ADCP data from the slope is upward propagation of phase, which is seen at both seasonal and intraseasonal time scales; on a few occasions, however, the phase propagates downward as well (Mukherjee et al., 2014; Amol et al., 2014).

The ADCP data from the east-coast shelf have not yet been described, unlike on the west coast (Amol et al., 2012, 2017; Amol, 2014), save for the near-inertial currents (Mukherjee et al., 2013). The shelf in the BoB is a data-sparse region and little is known about the circulation here. Shetye et al. (1991) showed a 40 km wide upwelling band hugging the shelf during the summer monsoon of July–August 1989 and pointed to the possible existence of shelf waves with an alongshore wavelength of 400–500 km, but there has been no confirmation of these observations using other data. Unfortunately, the altimeter data are not reliable in the vicinity of the coast and the narrow width of the east-coast shelf implies that even the along-track data of Durand et al. (2009) do not extend onto the continental shelf.

Though the ADCP data provide unprecedented information on the variability of the EICC, they suffer from three disadvantages. First, measurements on the shelf are restricted to the outer shelf as the threat to the moorings from fishing activity is considerable closer to the coast. Second, these are sub-surface moorings and the data are not available near the surface: the data lost owing to the echoes from the surface is roughly 10% of the range, which is around 40 m on the slope (Mukherjee et al., 2014; Amol et al., 2014) and 15–20 m on the shelf (Amol et al., 2012). Third, since the moorings are serviced once a year and do not include a surface buoy for real-time data transmission, the data are not available in real time.

One way to make continuous measurement of the surface current in near-real time is to use high-frequency (HF) coastal radars; since they are deployed on land, they are not threatened by fishing craft, unlike moored surface buoys deployed on the nearshore shelf. A pair of radars deployed on the coast can provide surface-current data at a temporal resolution of one hour and a spatial resolution of 6 km × 6 km over a patch of the sea spanning about 150 km × 150 km (Paduan and Washburn, 2013). In this paper, we use HF radar data for a few months

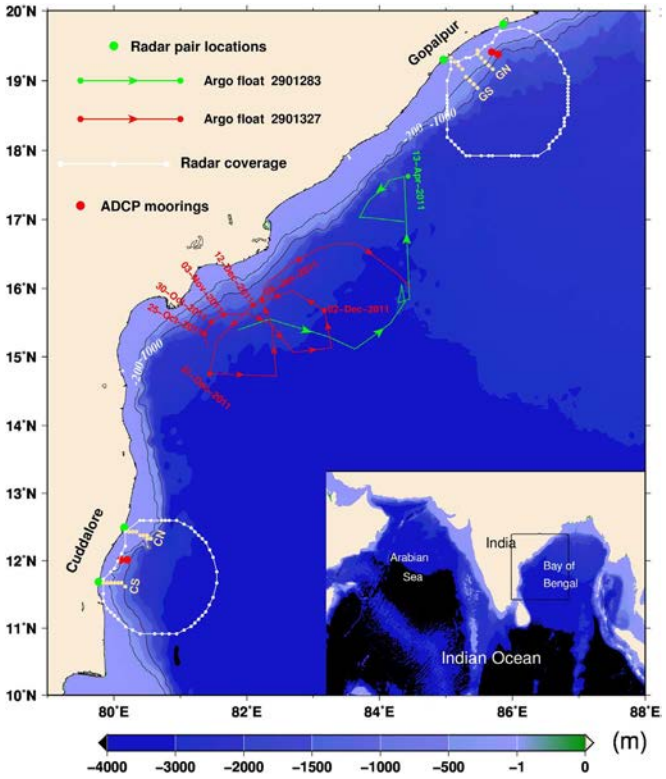

Fig. 1. The region of interest, the Bay of Bengal, and its location in the larger region (inset). The colour scale shows the bathymetry (metres). The 200 m (shelf break) and 1000 m contours are overlaid. The radar stations are depicted by the big solid green circles and the ADCP locations by the big solid red circles. The white curve with the soild white circles marks the limit of the radar coverage once GDOP (30–150° angle criterion; (Chapman et al., 1997)) is taken into account. The small solid yellow circles mark the cross-shore sections used to evaluate the cross-shore correlation of the surface EICC (Fig. 12); the correlation is estimated with respect to the location farthest from the coast, leading to an auto-correlation of 1 for this location. The tracks of the two Argo floats used to estimate the changes in the depth of the mixed layer are depicted by the green and red curves; the solid circles of the same colour mark the location at which the profile was selected. The profiles of temperature and salinity are plotted in Fig. 9 using the same colour as used here for the float trajectory.

Table 1
Location of HF radars used in this study and the period over which data are available from these radars. Though Odisha (Tamil Nadu) is the northern (southern) state in which the radars near Gopalpur and Puri (Cuddalore and Kalpakkam) are deployed, we use "Gopalpur" and "Cuddalore" to refer to the northern and southern radar pairs to match the nomenclature used for the ADCPs by Mukherjee et al. (2014). Data at Gopalpur (Cuddalore) are available for ~7 months (~5.5 months).

State	Towns	Location	Data period
Odisha	Puri Gopalpur	85.86°E, 19.80°N, 84.96°E, 19.30°N	23-August-2011 to 24-March-2012
Tamil Nadu	Cuddalore Kalpakkam	79.77°E, 11.68°N 80.15°E, 12.49°N	12-July-2011 to 30-December-2011

during 2011–2012 from the northern and southern parts of the Indian east coast; these data are based on observations made using two pairs of HF radars deployed by the National Institute of Ocean Technology (NIOT), Chennai. Unfortunately, not much work has been done with these current data because of numerous gaps, which make it difficult to carry out analysis using standard tools. These gaps preclude, for example, the computation of a reliable spectrum using Fast Fourier Transforms (FFTs) or wavelets. While nothing can be done to fill the long gaps of the order of a month or more (unless the time scale of interest is much greater than the gap length), there are several shorter gaps of the order of a few days, which can be filled. Filling these short

Table 2
Data gaps in the HF radar records from Gopalpur (Odisha pair) and Cuddalore (Tamil Nadu pair). The data gaps of 14 h or less are filled using linear interpolation and the method described in supplementary is used to fill the these longer gaps.

Sr. No.	Data gaps (missing data)	Span of the gap
Gopalpur: August 2011 to March 2012		
1	12/10/2011 12:00–13/10/2011 09:00	22 h
2	16/10/2011 07:00–17/10/2011 05:00	23 h
3	27/10/2011 09:00–27/10/2011 23:00	15 h
4	05/11/2011 23:00–08/11/2011 10:00	60 h
5	08/11/2011 17:00–09/11/2011 11:00	19 h
6	12/11/2011 17:00–13/11/2011 09:00	17 h
7	25/11/2011 00:00–02/12/2011 20:00	7 days 20 h
8	03/12/2011 12:00–04/12/2011 08:00	21 h
9	15/12/2011 15:00–20/12/2011 18:00	5 days 4 h
10	02/01/2012 16:00–03/01/2012 11:00	20 h
11	20/01/2012 07:00–20/01/2012 22:00	16 h
12	21/01/2012 06:00–23/01/2012 17:00	60 h
13	20/02/2012 20:00–23/02/2012 02:00	55 h
14	24/02/2012 00:00–28/02/2012 21:00	4 days 22 h
15	07/03/2012 01:00–07/03/2012 18:00	18 h
16	10/03/2012 23:00–11/03/2012 22:00	24 h
17	12/03/2012 01:00–12/03/2012 18:00	18 h
18	18/03/2012 07:00–18/03/2012 22:00	16 h
19	19/03/2012 07:00–19/03/2012 22:00	16 h
20	22/03/2012 07:00–22/03/2012 21:00	15 h
Cuddalore: July 2011 to December 2011		
1	13/09/2011 14:00–16/09/2011 15:00	74 h
2	02/10/2011 08:00–03/10/2011 17:00	34 h
3	10/10/2011 10:00–13/10/2011 02:00	65 h
4	18/11/2011 10:00–22/11/2011 03:00	90 h
5	03/12/2011 12:00–04/12/2011 07:00	20 h
6	06/12/2011 11:00–08/12/2011 11:00	49 h
7	12/12/2011 07:00–12/12/2011 21:00	15 h
8	19/12/2011 07:00–27/12/2011 02:00	7 days 20 h

gaps will make the data continuous over a few months, permitting an analysis of the variability. Without filling these gaps, all that can be done is to use the data to make spatial maps for a given time: an example of such an analysis is shown in John et al. (2015), who used the HF radar data to show what happened on 8 October 2015 in the vicinity of the Andaman and Nicobar Islands (India) during Cyclone Phailin.

In the Supplementary Material, we present a method for filling the short data gaps of the order of a few days and use the resulting, continuous time series of spatial maps of the surface current to describe the EICC. There exist reports of comparison of HF radar data with data from Lagrangian drifting buoys (Kuang et al., 2012; Rohrs et al., 2015), high-resolution surface drifters (Ohlmann et al., 2007), current meters (Emery et al., 2004), and ADCPs (Emery et al., 2004; Cosoli et al., 2010; Robinson et al., 2011). No such study is available, however, for the currents measured by the Indian HF radars.

We compare the data from these HF radars with the ADCP data from the slope (Mukherjee et al., 2014) and shelf off the Indian east coast and show that there are instances when the phase does not propagate all the way to the surface owing to the shallow mixed layers typical of the bay. The shallowness of the surface mixed layer leads to a strong vertical shear of the alongshore current. The HF radar data also show that the EICC, which is essentially a boundary current forced by basin-scale processes (McCreary et al., 1996; Shankar et al., 2002), leaves its imprint on the nearshore current.

The paper is organised as follows. We present the data sources and model description in Section 2 and describe the temporal variation of the EICC at the ADCP locations in Section 3 and the spatial variation in Section 4. The results are discussed in Section 5, which includes a comparison with a simulation of the EICC using a state-of-the-art oceanic general circulation model (OGCM), and Section 6 concludes the paper.

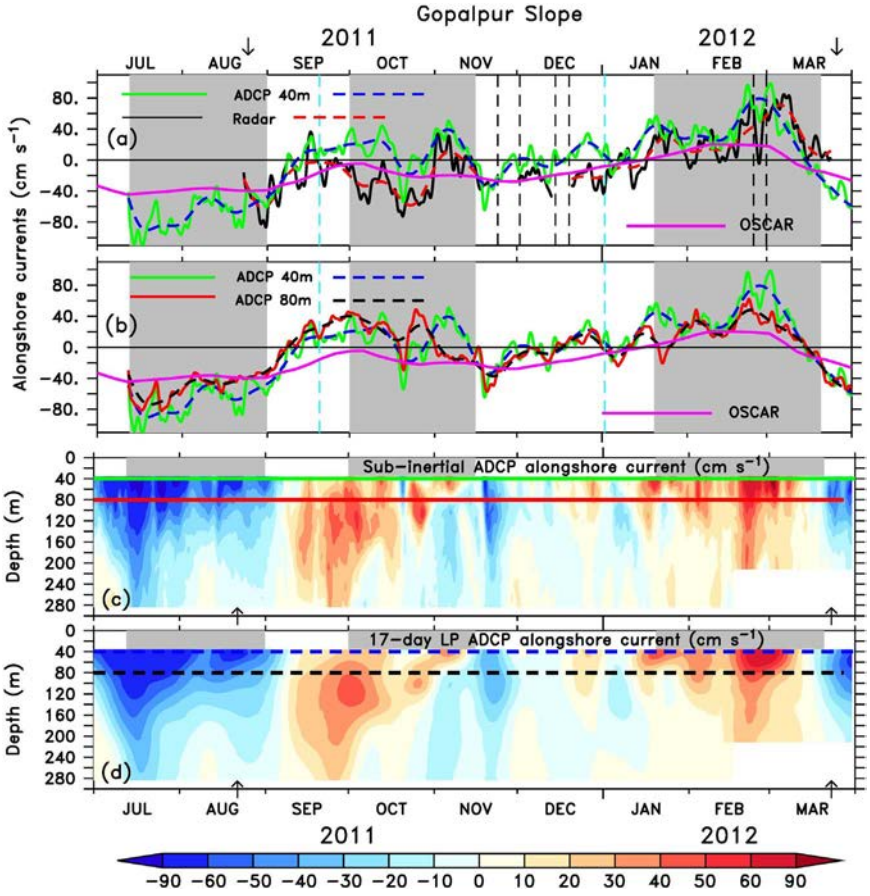

Fig. 2. (a) HF radar, ADCP (40 m), and OSCAR alongshore currents (cm s^{-1}) off Gopalpur on the slope. The solid curves represent the sub-inertial currents and the dashed curves the 17-day low-pass-filtered currents. The sign convention is that the poleward current (upwelling favourable) is positive. The vertical, black dashed, line pairs represent the major gaps in the radar data (Table 2) and the dashed, cyan vertical lines represent the duration of the equatorward burst. The grey background marks the period over which the averaging was carried out for the vertical profile of currents shown in Fig. 18; the vertical profiles are shown for three seasons. (b) As in (a), but for the ADCP (40 m and 80 m) and OSCAR currents. (c) The sub-inertial ADCP current as a function of depth (m; ordinate) and time (Indian Standard Time or IST, which is UTC + 05:30; abscissa). The 40 m and 80 m depths are marked by the horizontal lines. (d) As in (c), but for the 17-day low-pass-filtered ADCP current. The vertical arrows at the top or bottom of some panels mark the beginning and end of the radar record for the station. Note that the OSCAR current is the same for both shelf and slope owing to the coarse resolution of these data and the narrow shelf off the Indian east coast.

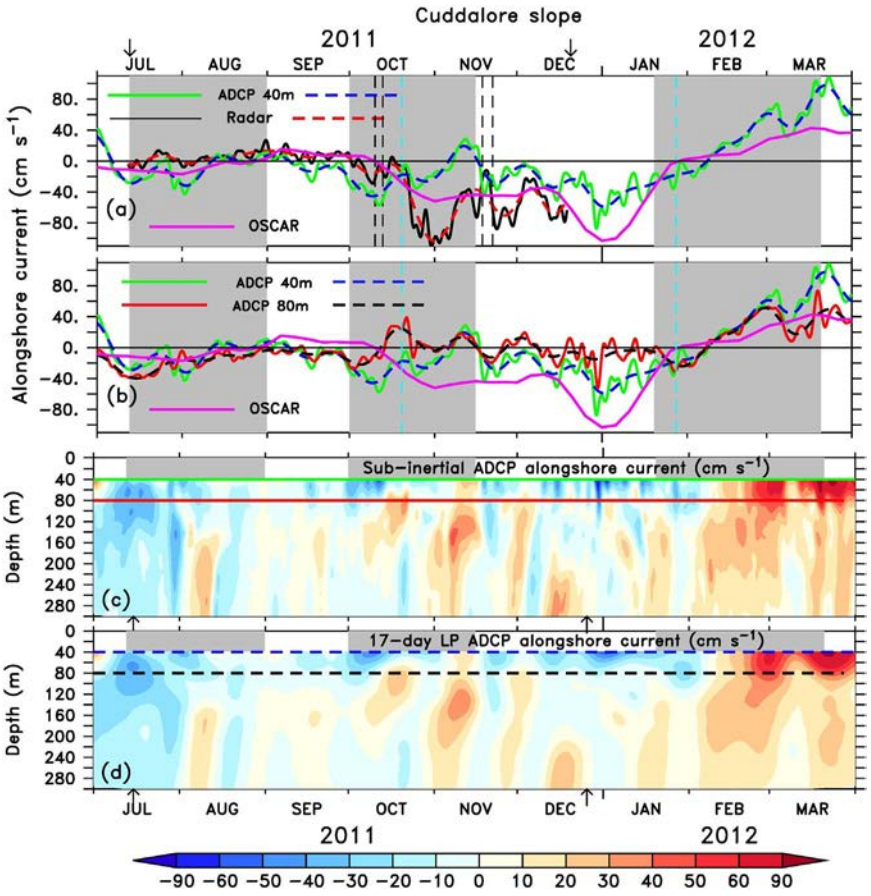

Fig. 3. Same as Fig. 2, but for Cuddalore.

Table 3
Root mean square (RMS) and standard deviation of the alongshore current V (cm s^{-1}) measured by the HF radar and ADCPs. V_R denotes the radar current and V_{A20} and V_{A40} denote the ADCP currents at 20 m and 40 m, respectively.

Alongshorecurrent current		Gopalpur		Cuddalore	
		SD	RMS	SD	RMS
Shelf	V_R	35.22	36.37	26.57	30.59
	V_{A20}	28.68	28.71	27.00	32.06
	V_{A40}	26.78	28.06	14.53	18.16
Slope	V_R	34.37	35.23	35.60	41.43
	V_{A40}	30.95	32.89	17.29	22.16

2. Data and model

We use data from HF radars located on the Indian east coast and ADCPs moored on the shelf and slope off the east coast. In addition, we use current estimates from the OSCAR (Ocean Surface Current Analyses Real-time) product, sea-level-anomaly (SLA) data from the altimeter, and temperature and salinity data from Argo floats. We also use an OGCM known as Modular Ocean Model (MOM) to simulate the EICC. The data and model are briefly described in this section.

2.1. ADCP data

The ADCP data are from a mooring each on the shelf and slope off Gopalpur (~19°N) and Cuddalore (~12°N) (Fig. 1); the slope data were described by Mukherjee et al. (2014). The slope moorings were deployed at a water-column depth of ~1100 m, with the 75 kHz ADCP located at ~300–350 m, implying a loss of data in the top ~40 m from the surface; the bin size was 8 m and the sampling interval one hour. The shelf mooring off Gopalpur (Cuddalore) was deployed at a water-column depth of ~180 m (~100 m), with the 150 kHz (300 kHz) ADCP located just above the acoustic release near the bottom of the mooring. For the shelf moorings, data were not available in the top 15 m (20 m) off Gopalpur (Cuddalore); the bin size was 4 m and the sampling interval 15 min.

Following Mukherjee et al. (2014), the tidal components with a period equal to or less than a day were removed using the TASK-2000 software (Bell et al., 1998) and, following Amol et al. (2012), the gaps in the ADCP data in depth and time were filled using the methods of Kutsuwada and McPhaden (2002). A low-pass filter with a cutoff of 50 h (75 h) was used for the ADCPs off Gopalpur (Cuddalore). All filters used in this paper are fourth-order, Butterworth filters. We use all the available data from July 2011 to March 2012 for all four ADCPs; data are not available off Cuddalore after 10 February 2012. Mukherjee et al. (2014) used the data from the slope ADCPs for 2009–2013 to describe the observed seasonal and intraseasonal variability of the EICC. The data from the shelf ADCPs have not been used yet to describe the sub-inertial EICC.

2.2. HF radar data

Five pairs of HF radars of make CODAR (Coastal Ocean Dynamics Applications Radar) have been installed by NIOT in the Indian waters. One radar pair is located in the Andaman Islands (John et al., 2015) and one in the Gulf of Khambhat on the west coast of India. Three pairs, with a transmitting frequency of 4.4 MHz (John et al., 2015), are located on the Indian east coast. This distribution of the radar systems, with a bias towards the Indian east coast, is due to them being funded as part of the tsunami warning system at the Indian National Centre for Ocean Information Services (INCOIS). The data are received at both INCOIS and NIOT and data for a few months during 2011–2012 were

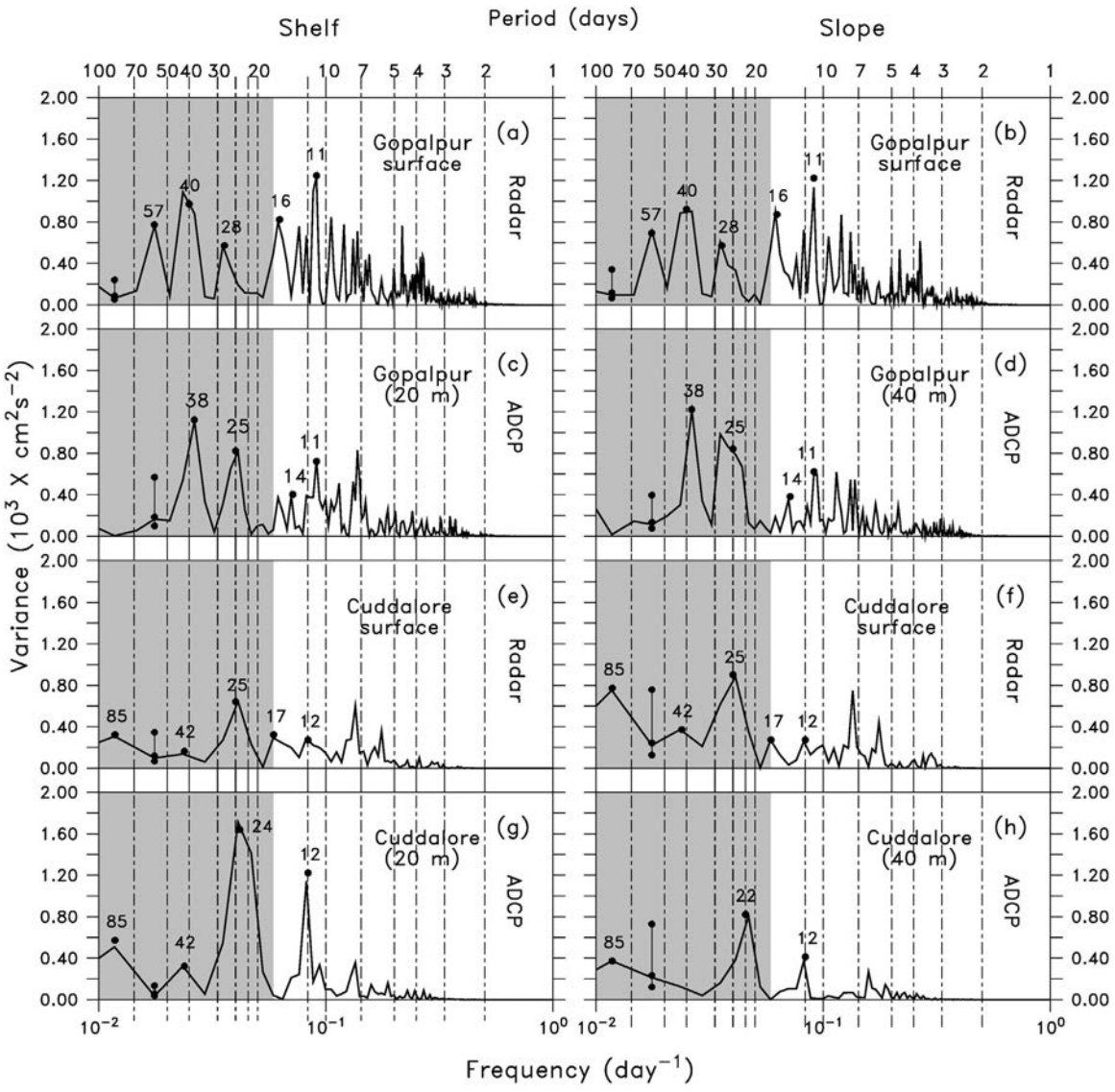

Fig. 4. Variance preserving spectrum (FFT) for radar and ADCP alongshore currents on the shelf (left panels: a, c, e, g) and slope (right panels: b, d, f, h). The top (bottom) two panels are for the EICC off Gopalpur (Cuddalore), with the upper (lower) panel in each set representing the spectrum for the radar (ADCP) current. The ADCP bin is at 20 m (40 m) on the shelf (slope). The spectra were generated after applying a 75% Tukey window to the detided data. The vertical bars with solid circles near the left bottom corner of each panel represent the confidence intervals for the spectrum. In computing the spectrum for the ADCP current, we used the data for the period 12 July 2011 to 24 March 2012, i. e., from the beginning of the Cuddalore radar record to the end of the Gopalpur radar record (Table 1). The shading is used to mark the periods greater than or equal to 17 days, the cut-off used for the low-pass filter.

made available to us for two radar pairs on the east coast. These data are from the northern and southern parts of the coast. We refer to the northern (southern) radar data as “Gopalpur” (“Cuddalore”); this nomenclature was used for the ADCPs by Mukherjee et al. (2014) and is based on the major towns located in the area. The data from the third pair, located on the central east coast, had far too many gaps to permit analysis. The location of these radars is shown in Fig. 1 and Table 1.

The current data were provided by INCOIS in the form of hourly snapshots of the surface current for the region covered by a radar pair. The data made available were already decomposed into earth coordinates following processing of the radial current measured by the radars. In processing the data, one has to account for the geometric dilution of precision (GDOP), which is treated as a baseline uncertainty problem in the estimated vector current near the baseline joining the two radar stations; to reduce the error due to GDOP, the total vector is considered reliable only when the angle between the radials from the two sites is within the range 30–150° because it is within this range that the error due to GDOP is small enough (Chapman et al., 1997). This GDOP effect was taken care of in processing the data: the area over which the current data were considered reliable is shown in Fig. 1.

We detided the current data using the Tidal Analysis Software Kit (TASK; Bell et al., 1998) and all the tidal constituents with a period of a day or less were removed. Further analysis was carried out with these hourly data. While TASK can work with gappy data, further analysis demands a continuous data set, for which we had to fill several gaps in the HF radar data. The method used is described in the Supplementary Material, which also shows that the method has a much weaker impact on the wavelet spectrum compared to linear interpolation or cubic splines. Following the filling of these gaps, we used low-pass filters to retain only the sub-inertial component of the current. For the Gopalpur (Cuddalore) radar currents, we used 17 °N (10 °N) as the southern boundary, implying a cut-off of 50 h (75 h). It is these de-tided, sub-inertial currents that we describe in this paper.

The current vectors were rotated to obtain alongshore and cross-shore components for comparison with the ADCP data; the rotation angles and method are as given in Mukherjee et al. (2014) for the ADCP data. Poleward (upwelling favourable) and offshore current components are considered positive.

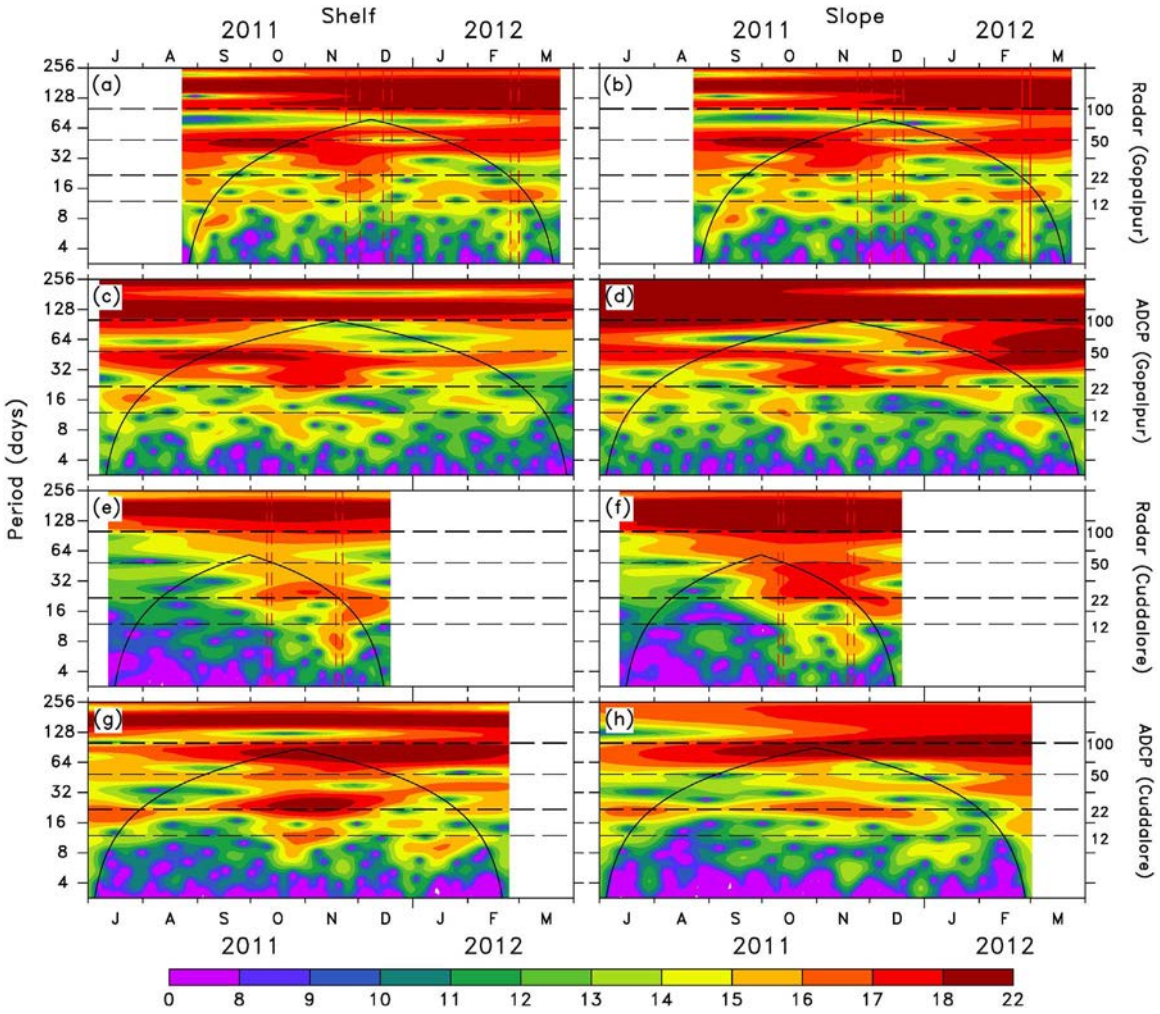

Fig. 5. The distribution of panels is as in Fig. 4, but this figure shows the wavelet power spectrum ($cm^2 s^{-2}$) as a function of time (abscissa) and period (ordinate). The thick and continuous black line shows the cone of influence. The ordinate and the wavelet power are plotted on a $\log_2$ scale. Note that the contour interval is not uniform. The horizontal dashed lines mark 12, 22, 50, and 100 days on the ordinate. The vertical pairs of red lines mark the bigger gaps in the radar data (Table 2).

2.3. Satellite data

OSCAR uses satellite data to generate ocean surface velocities; the surface currents are provided on a global grid approximately once every five days and the data are available from 1992 onwards (Bonjean and Lagerloef, 2002). The data are freely available through two data centres operated by National Oceanic and Atmospheric Administration (NOAA) and National Aeronautics and Space Administration (NASA). The NASA site http://podaac.jpl.nasa.gov/ serves OSCAR current data on both 1° and $\frac{1}{3}$° grids. We compare the finer-resolution OSCAR current, which represents an average over the top 30 m, with the HF radar current, which is representative of the surface current. Comparison with the slope ADCP data shows that the OSCAR current often lags the ADCP current in the topmost bin (40 m) on the slope owing to the upward propagation of phase, but the OSCAR current estimate is otherwise a good measure of the near-surface flow measured by the ADCP (Amol et al., 2014; Mukherjee et al., 2014).

We also use SLAs from the altimeter (AVISO, 1996) to compare with the spatial current maps generated by the HF radar. The SLA data were downloaded from http://www.aviso.oceanobs.com/duacs/.

2.4. Argo data

For estimating the depth of the mixed layer in the EICC regime, we use vertical profiles of temperature and salinity from two Argo floats. The Argo float positions and tracks are shown in Fig. 1. These data were downloaded from http://www.argodatamgt.org/Access-to-data/Argo-data-selection.

2.5. The ocean model

To simulate the EICC, we use an oceanic general circulation model (OGCM) called Modular Ocean Model (MOM; Griffies, 2009). The specific version used is MOM4p1 and the model setup is described in detail in Chatterjee et al. (2017) and Mukherjee et al. (2017). We give but a brief summary here; the simulation used in this paper is the control run of Mukherjee et al. (2017).

MOM is a Boussinesq, hydrostatic, free-surface ocean model; it uses the Arakawa-B grid for the horizontal orthogonal coordinates and has a generalized depth coordinate with the minimum depth set to 15 m. Our model domain is 30 °S to 30 °N and 30–120°E and the resolution is 0.1° × 0.1°. The model has 40 vertical levels, with a resolution of 5 m in the top 60 m. The bottom topography is taken from the modified 2′ bathymetry of Sindhu et al. (2007). The narrow channel between India and Sri Lanka is closed and the channels connecting the Persian Gulf and Red Sea with the Arabian sea are deepened and broadened to allow flow through them; the South China Sea is masked out of the model domain. A sponge layer of 3.5° has been applied along the open boundaries of the south and east (Chatterjee et al., 2013) and the no-slip condition to continental land boundaries. Surface salinity is relaxed

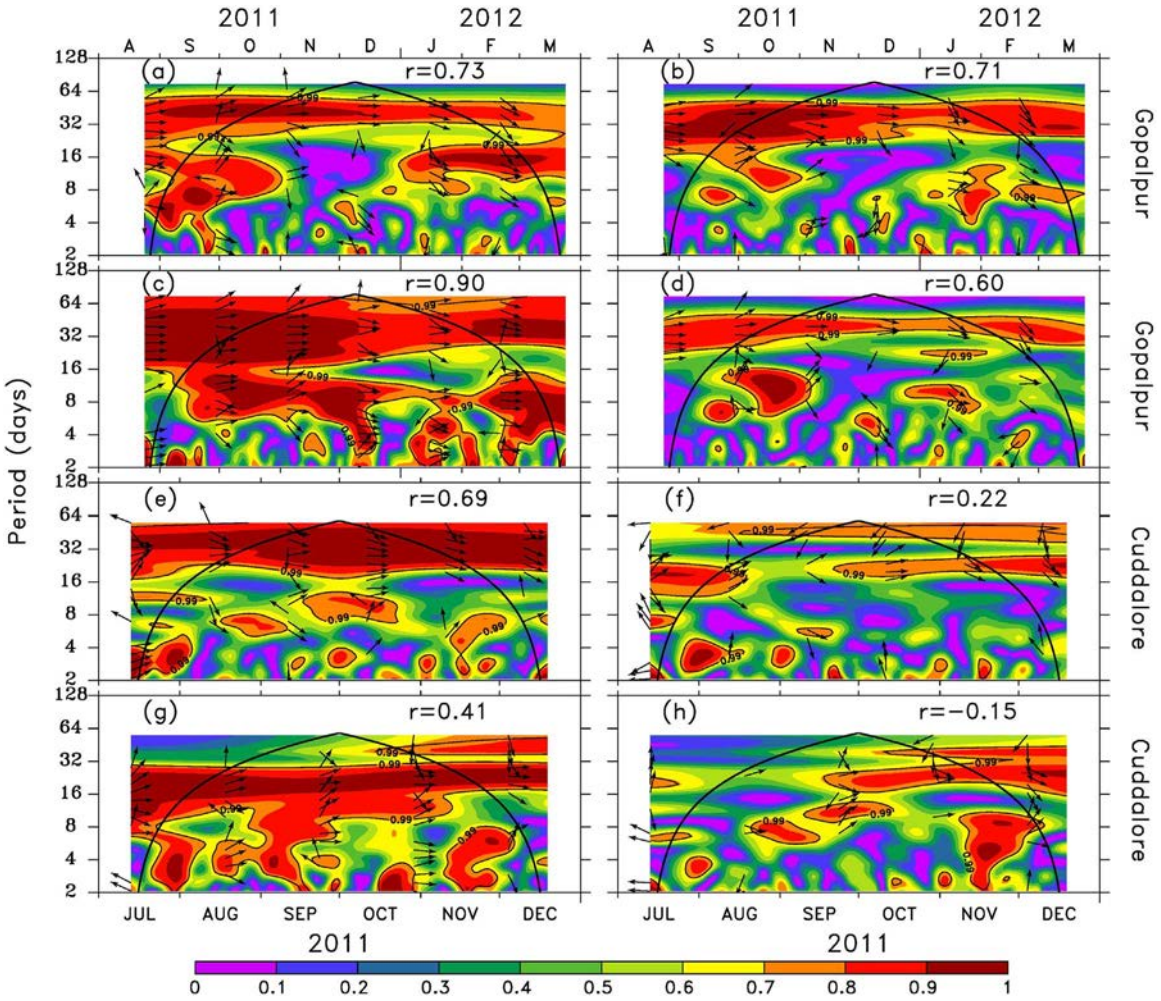

Fig. 6. Wavelet coherence between the radar and ADCP currents at the ADCP mooring locations. The wavelet coherence, unlike the correlation that is written in each panel, provides a measure of the correlation as a function of time and period. The thick black curve denotes the cone of influence and the coherence above the 99% significance level is marked by the black contour. (a) Correlation and coherence on the shelf between the radar and 20 m ADCP current off Gopalpur. (b) Correlation and coherence on the slope between the radar and 40 m ADCP current off Gopalpur. (c) Correlation and coherence on the shelf between the 20 m and 40 m ADCP currents. (d) Correlation and coherence on the shelf between the radar and 40 m ADCP currents. (e) As in (a), but for Cuddalore. (f) As in (b), but for Cuddalore. (g) As in (c), but for Cuddalore. (h) As in (d), but for Cuddalore.

to the monthly climatological values of Chatterjee et al. (2012). The wind forcing in the model is taken from daily ASCAT scatterometer and radiation fluxes from the NCEP/NCAR (National Centers for Environmental Prediction / National Center for Atmospheric Research) reanalysis product (Kalnay et al., 1996).

3. Temporal variation of the EICC

The ADCP data show the temporal variation of the EICC. In this section, we compare the HF radar data at the ADCP locations with the ADCP and OSCAR currents. We restrict our attention to the alongshore current. As noted in Section 2, the currents have been filtered with a 50-h (75-h) low-pass filter for Gopalpur (Cuddalore) to retain only the sub-inertial component. Since the slope EICC during 2009–2013 has been described by Mukherjee et al. (2014), we begin with a description of the radar data on the slope, followed by the shelf. In making this comparison between the radar current and ADCP or OSCAR current, we pick the radar point or OSCAR grid nearest the ADCP location. The coarse resolution of the OSCAR product (0.33°) implies that we get the same grid cell for both slope and shelf locations. The section ends by relating the observed vertical shear to the depth of the surface mixed layer.

3.1. The slope EICC

The topmost ADCP bin for which data are available on the slope is at 40 m. Hence, we compare the ADCP current at 40 m and 80 m (the lowest common depth bin for the shelf ADCPs) with the radar and OSCAR currents .

The OSCAR current varies fairly smoothly and shows the expected temporal variation. Off Gopalpur (Fig. 2a), the OSCAR data show that the EICC flows equatorward from July–December 2011, poleward during January–March 2012, and equatorward again at the end of March. The ADCP current does not match this variation even at 40 m: it is equatorward during July–August 2011 and largely poleward during September–October, but with a strong equatorward burst in the middle of October. The radar data are available from 23 August 2011 onwards (Table 1) and match the ADCP data during August, but not during September–October, when the surface (sub-surface) EICC flows equatorward (poleward). The equatorward EICC is shallow, except for the burst during mid-October, which appears as a deep flow extending from the surface to over 80 m (Fig. 2a–c). The equatorward EICC later in November also extends from the surface to 80 m, but the EICC reverses earlier at 40–80 m (Fig. 2c) than at the surface, where the poleward flow sets in only during January (Fig. 2a), a lag of over a month compared to the 40 m ADCP current. The ADCP currents at 40 m and 80 m tend to be in the same direction off Gopalpur (Fig. 2b,c). The RMS

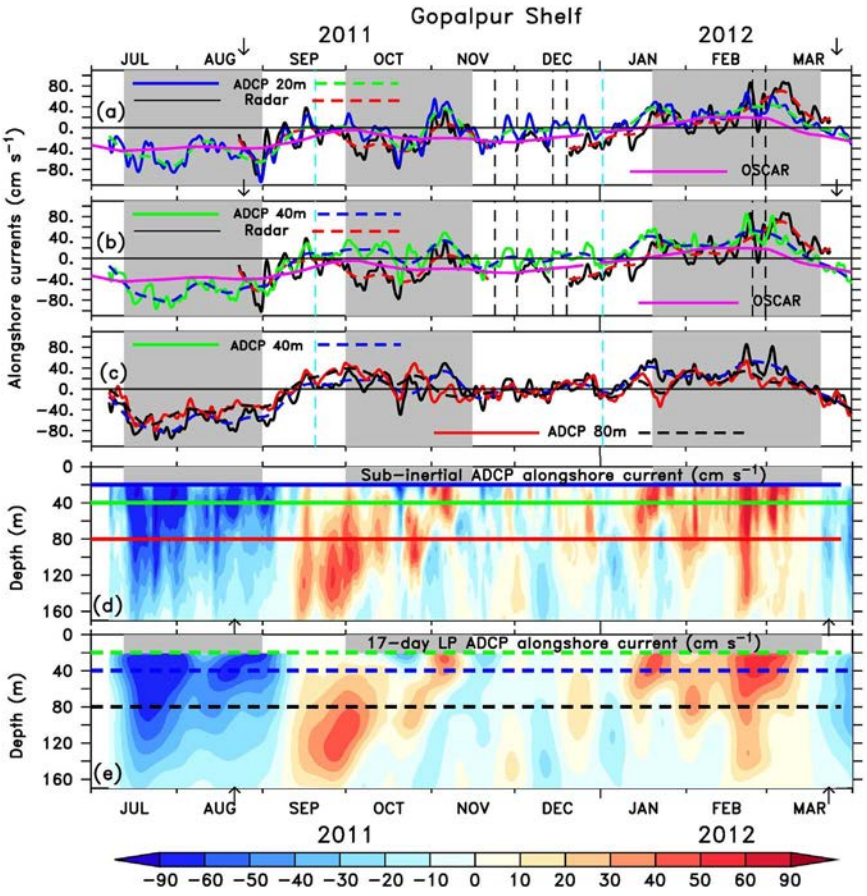

Fig. 7. (a) HF radar, ADCP (20 m), and OSCAR alongshore currents (cm s^{-1}) off Gopalpur on the shelf. The solid curves represent the sub-inertial currents and the dashed curves the 17-day low-pass-filtered currents. The sign convention is that the poleward current (upwelling favourable) is positive. The vertical, black dashed, line pairs represent the major gaps in the radar data (Table 2) and the dashed, cyan vertical lines represent the duration of the equatorward burst. The grey background marks the period over which the averaging was carried out for the vertical profile of currents shown in Fig. 18; the vertical profiles are shown for three seasons. (b) As in (a), but for the radar, OSCAR, and 40 m ADCP currents. (c) As in (c), but for the ADCP (40 m and 80 m) currents; the OSCAR and radar currents are not plotted in this panel. (d) The sub-inertial ADCP current as a function of depth (m; ordinate) and time (Indian Standard Time or IST, which is UTC + 05:30; abscissa). The 20 m, 40 m, and 80 m depths are marked by the horizontal lines. (e) As in (d), but for the 17-day low-pass-filtered ADCP current. The vertical arrows at the top or bottom of some panels mark the beginning and end of the radar record for the station. Note that the OSCAR current is the same for both shelf and slope owing to the coarse resolution of these data and the narrow shelf off the Indian east coast.

(root mean square) and standard deviation of the alongshore EICC are comparable for the radar and ADCP data at 40 m, but the OSCAR current tends to be weaker than the radar current even though both tend to show the same direction (Table 3, Fig. 2a,b).

Off Cuddalore, the OSCAR data show that the EICC is weak during July–September (Fig. 3a). It flows equatorward during October–December, with a peak in December, before reversing to flow poleward in January as the seasonal, sub-tropical gyre begins to form in the Bay of Bengal (Shetye et al., 1993). The ADCP and radar current are also weak during July–September, with reversals occurring over both depth and time. From October–December, the radar current is equatorward, like the OSCAR current, but the ADCP current at 80 m (Fig. 3b) tends to reverse direction a few times and even the current at 40 m reverses direction twice, flowing persistently equatorward only from mid-November to the end of January. This difference in direction between the surface and 40 m current is reflected in the strikingly different values of the RMS and standard deviation of the current at these depths (Table 3) and in the lower correlation between the surface and 40 m current at Cuddalore ($r = 0.22$, but still significant at the 99% level) compared to Gopalpur ($r = 0.71$). The radar data are not available after December, when both OSCAR (Fig. 3a) and ADCP (up to 80 m; Fig. 3c) show poleward flow. Given the good match between the direction of the OSCAR and radar currents, however, it is likely that the surface EICC is poleward at this time.

Unlike the smooth variation of the OSCAR current, the radar and ADCP currents show considerable variation at higher frequencies (Figs. 2, 3). A Fast Fourier Transform (FFT) shows periodicities of 11–17 days, around 22–28 days, and ~38–42 days at Gopalpur and Cuddalore and a weaker peak around 85 days at Cuddalore (Fig. 4, right panels). The band around 12 days (11 days) and 16 days (17 days) is strong (weak) on the slope off Gopalpur (Cuddalore), but these peaks are stronger off Gopalpur in the radar data. A wavelet transform (Fig. 5, right panels) shows that the 11–16-day variability off Gopalpur peaks in the neighbourhood of the data gaps, with the exception of the peak around 8–12 days during July–September. Though the gap-filling method reduces the error considerably, as shown in the Supplementary Material, the existence of these gaps does affect the FFT, the periodogram, and the wavelet power. This peak around 12 days is, however, also seen in the ADCP data (Fig. 4d,h, Fig. 5d,h) and in the longer ADCP data sets for both east (Mukherjee et al., 2014) and west (Amol et al., 2012, 2014) coasts of India, impplying that it is a signal, not an artefact of the data gaps. This 12-day peak on the east coast is stronger for the poleward flow associated with the seasonal, subtropical gyre (Shetye et al., 1991) during February–May (see Figs. 5 and 9 in Mukherjee et al., 2014). The coverage of the radar data set available to us is limited and does not extend into this season (Table 1); hence, the strong intraseasonal peaks around ~12 days are seen during the summer monsoon off Gopalpur and October–December off Cuddalore (Figs. 2, 3, 5).

The other peaks in the FFT are common to both radar and ADCP currents, but the peak around 42 days (Fig. 4, right panels) or the band between 25 and 40 days (Fig. 5, right panels) are exceptions. These two peaks are present in the radar current off Cuddalore (Fig. 4f, but absent in the ADCP current at 40 m (Fig. 4h). The FFT and the wavelet analyses show that both radar and ADCP data contain more variability around 22–25 days off Cuddalore; off Gopalpur, it is the variability around 38–40 days that is stronger. Hence, we see more high-frequency variability in the current data off Cuddalore (Fig. 3a,c) than off Gopalpur (Fig. 2a,c). The ~25-day peak is not, however, associated with the data gaps; hence, we retain this periodicity while eliminating the higher frequencies with a 17-day low-pass filter.

The filtered data show that the OSCAR current tends to produce an average between the surface current measured by the HF radar and the ADCP current at 40 m (Figs. 2, 3). Striking in this low-passed ADCP

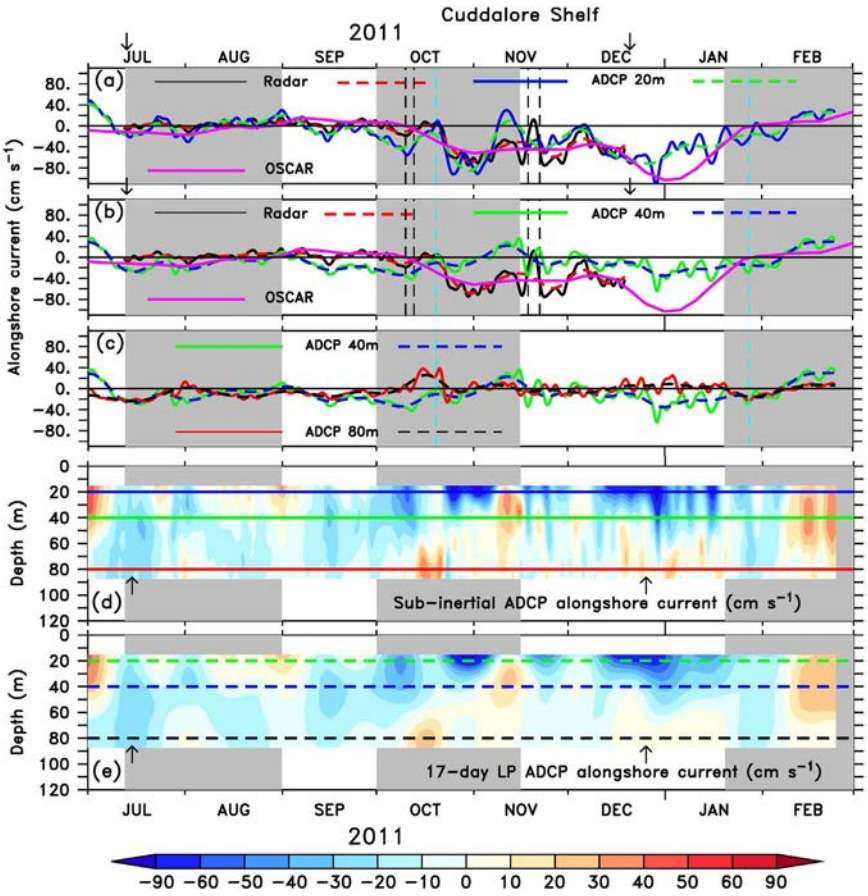

Fig. 8. Same as Fig. 7, but for Cuddalore.

current is the upward propagation of phase noted by Mukherjee et al. (2014). (Note that though the phase propagates upward most of the time, an example of downward phase propagation, also noted by Mukherjee et al. (2014), is seen during December–January off Cuddalore between ~40–120 m (Fig. 3d).) An example of upward phase propagation is the lag between the ADCP currents at 80 m and 40 m and between the ADCP current at 40 m and the radar current during February–March 2012 off Gopalpur (Fig. 2a,d). There are occasions, however, when the upward phase propagation does not extend all the way to the surface. The strong poleward flow off Gopalpur between ~40–80 m during September–October 2011 (Fig. 2d) is not seen in the radar current (Fig. 2a). It is only towards the end of October that a higher-frequency burst propagates all the way to the surface, with a distinct lag between the curves at 80 m, 40 m, and the surface (Fig. 2b,a). This short-lived poleward burst, which succeeds the lower-frequency poleward burst during September–October, is evident in the ADCP data (Fig. 2d). Similarly, some of the high-frequency bursts during October–November 2011 in the ADCP current off Cuddalore (Fig. 3a,b,d) are not seen in the surface current, suggesting a shallow surface flow (associated with the EICC) that lowers the standard deviation and RMS of the current at 40 m (Table 3).

It is this difference between the sub-surface and surface currents at Cuddalore that leads to the absence (presence) of a weak peak around 42 days in the FFT for the ADCP (radar) current (Fig. 4h,f). This difference between the surface and 40 m currents at Cuddalore, evident in the low correlation and wavelet coherence between them (Fig. 6e), is also seen on the shelf and a discussion of the causes is therefore deferred till the shelf EICC is described. Off Gopalpur, as may be expected from the wavelet analysis (Fig. 5b,d), the correlation and wavelet coherence between the radar and ADCP (40 m) currents is high (Fig. 6a).

3.2. The shelf EICC

The shelf data for Gopalpur and Cuddalore are presented in Figs. 7 and 8, respectively. Though the topmost bin is at 20 m off Gopalpur and 15 m off Cuddalore, we present the data for 20 m for both locations; the Cuddalore data for 15 m are nearly identical to those for 20 m.

The radar current matches the ADCP current at 20 m well off both Gopalpur ($r = 0.74$; Fig. 6b) and Cuddalore ($r = 0.69$; Fig. 6f); both correlations are significant at 99%, suggesting low shear between the currents at these depths. As on the slope, however, the correlation on the shelf for the surface and 40 m currents, differs with location: the correlation off Gopalpur is still high ($r = 0.60$, statistically significant at the 99% level) and the wavelet spectra coherent (Fig. 6c), but the correlation is negative off Cuddalore ($r = -0.15$) and the wavelet spectra are not coherent (Fig. 6g). This shear between 0–20 m and 40 m at Cuddalore on both slope and shelf suggests a shallow surface EICC during October–December off southeast India (Fig. 8a–d). These correlations are consistent with the RMS and standard-deviation differences between the surface current and the current at 40 m on the slope and shelf off Cuddalore (Table 3), and, as expected, the coherence and correlations between the 20 m and 40 m shelf currents from the ADCP show a similar behaviour (Fig. 8a–d, Fig. 6h); in contrast, the shear is weaker at Gopalpur and the surface and 40 m currents are therefore more coherent (Fig. 7a–d, Fig. 6d).

Off Gopalpur, intraseasonal variability (~20–60 days) is comparable on the shelf and slope even if the depth of measurement on the shelf (slope) is 20 m (40 m; Fig. 5). Off Cuddalore, however, intraseasonal variability is stronger at 20 m on the shelf compared to 40 m on the shelf (figure not shown) or slope, suggesting a weakening of the intraseasonal variability with increasing depth. The variability in the radar currents is comparable for both locations. Another facet of this intraseasonal variability is that it extends over the entire record off

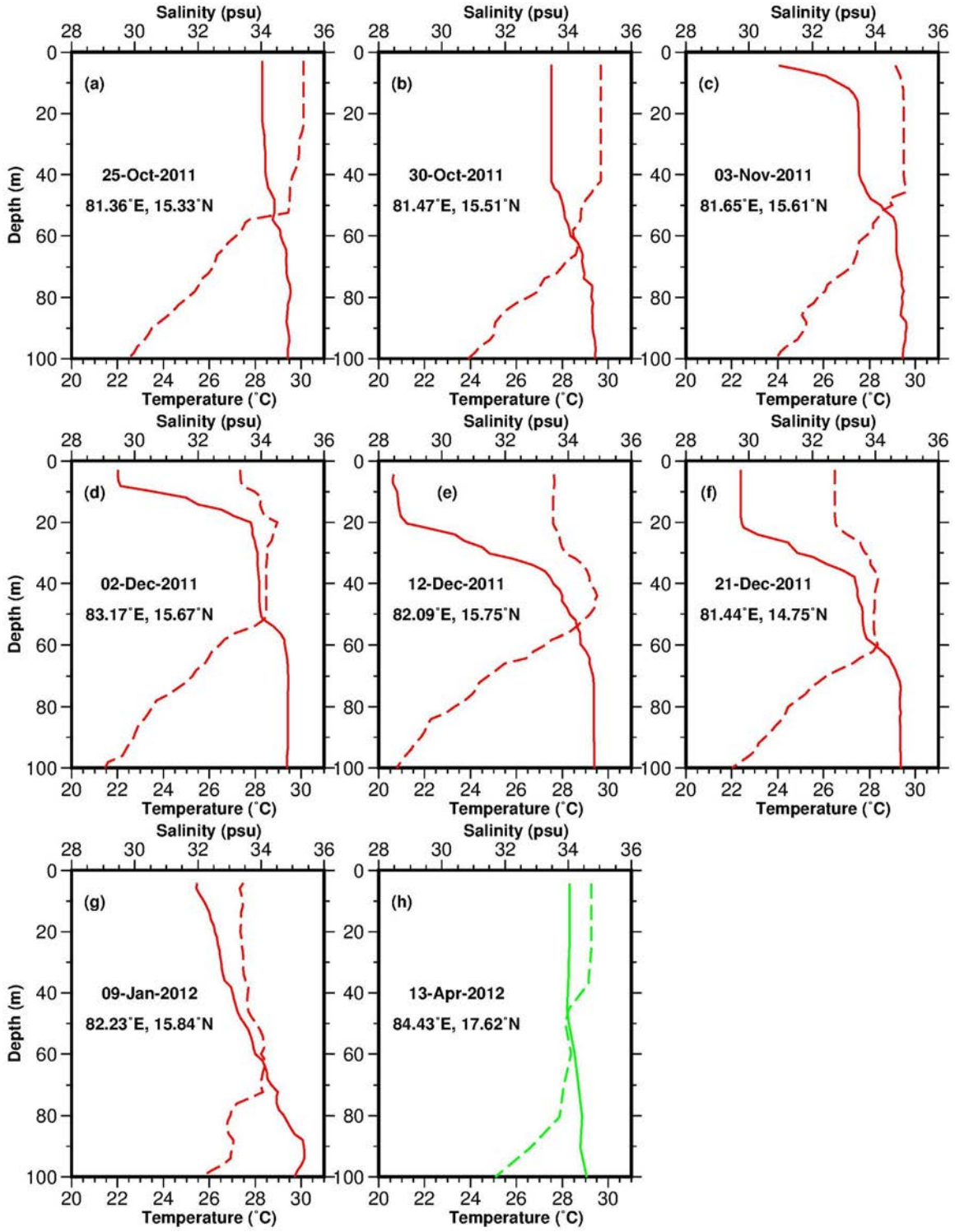

Fig. 9. Temperature (°C, dashed curves) and salinity (psu, solid curves) profiles as a function of depth (shown as pressure in decibars) from Argo floats 2901283 (green) and 2901327 (red) off the central east coast of India. The float trajectories are shown in Fig. 1 and the colour used for the profiles here is the same as used for the trajectory. The float locations and sampling date are also marked in Fig. 1.

Gopalpur, but is restricted to the equatorward burst during October–January off Cuddalore (Fig. 5).

Low-pass-filtering the data with a 17-day cutoff shows that upward phase propagation occurs on the shelf off both Gopalpur (Fig. 7e) and Cuddalore (Fig. 8e).

3.3. Vertical shear and the mixed layer

The literature suggests that the equatorward EICC during October–December is a shallow current (Shetye et al., 1996). Unfortunately, we do not have hydrographic data during October–December 2011 as no Argo floats traversed the region covered by the HF radars. Two floats did, however, sample the slope regime of the EICC between the two radar domains during October 2011 to April 2012

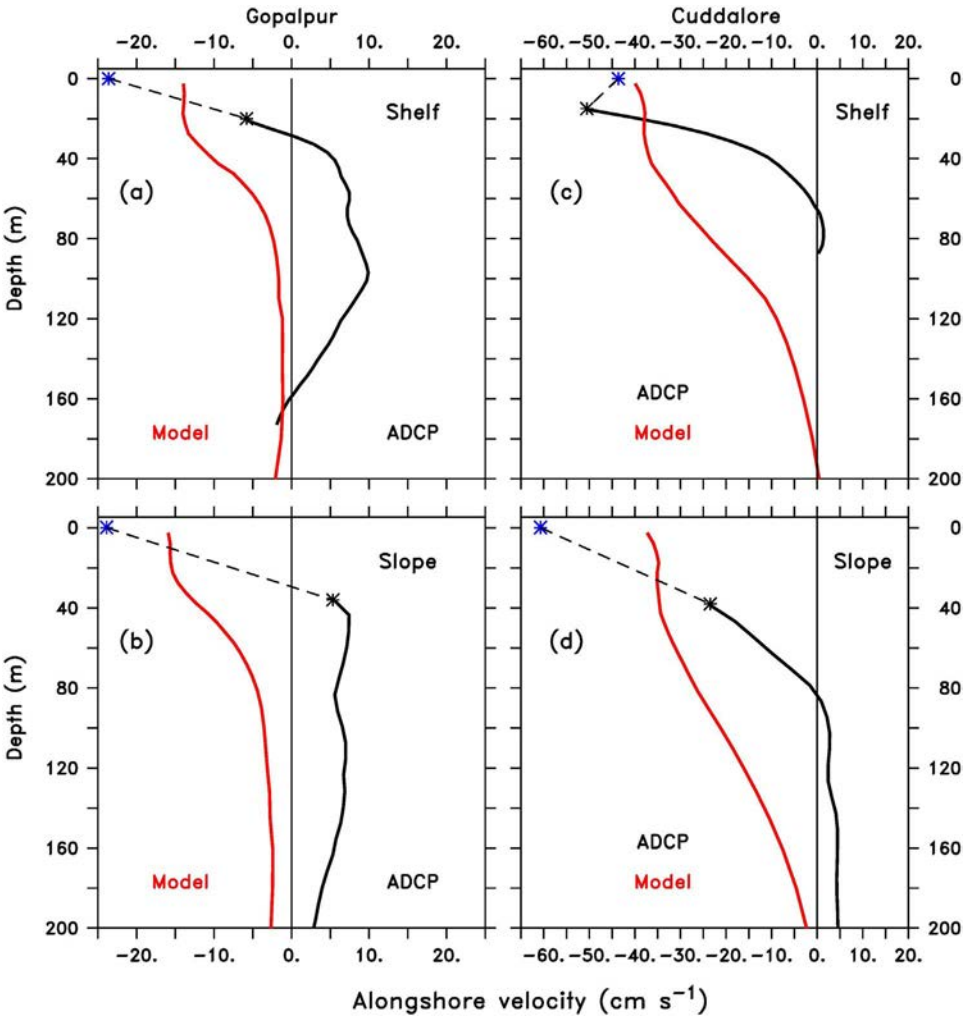

Fig. 10. Vertical profiles of alongshore currents (cm s^{-1}), averaged over the period of duration of equatorward burst in 2011, from observations and the MOM simulation on the shelf (top panels) and slope (bottom panels) for Gopalpur (left panels) and Cuddalore (right panels). The averaging period for Gopalpur (15-September-2011 to 15-December-2011) is denoted by the vertical cyan lines in Figs. 2 and 7; the averaging period for Cuddalore (20-October-2011 to 20-January-2012) is denoted by the vertical cyan lines in Figs. 3 and 8. The black asterisk represents the current in the topmost ADCP bin and the blue star the current from the HF radars. The data gap between the topmost ADCP bin and the surface is shown by the dashed line.

(Fig. 1) and we use these data to show the shallowing the surface mixed layer off the Indian east coast during the period of equatorward flow (October–December) off both Gopalpur (Figs. 2, 7) and Cuddalore (Figs. 3, 8).

The Argo profiles off the central east coast of India show a sudden shallowing of the mixed layer from ~40 m on 25 and 30 October (Fig. 9a,b) to ~15 m on 3 November owing to a shallow layer of low-salinity water (Fig. 9c). This shallowing of the mixed layer is not reflected in the temperature profile, which shows a barrier layer (Lukas, 1991; Vialard and Delecluse, 1998); such barrier layers have been noted in the hydrographic data from the western BoB during winter and they have been attributed to the equatorward advection of fresher water from the northern BoB (Shetye et al., 1996; Durand et al., 2007; Kurian and Vinayachandran, 2007). The mixed layer deepens gradually and the barrier layer erodes through November and December (Fig. 9d,e) till 21 December, when the barrier layer ceases to exist and the mixed layer is 20 m deep (Fig. 9f). The mixed layer continues to deepen (Fig. 9g) as the EICC reverses to flow poleward in January first in the northern bay (Figs. 2, 7) and then in the southern bay (Figs. 3, 8), cutting off the supply of the low-salinity surface water (Shankar, 1998, 2000; Han et al., 2001).

In contrast to the shallow mixed layer during November–December, the mixed layer is ~80 m deep in April (Fig. 9h), when a basin-wide gyre forms in the BoB, with a poleward EICC (Shetye et al., 1993; McCreary et al., 1993, 1996). The mixed layer shallows with the onset of the summer monsoon, when the local winds force a weak upwelling favourable EICC against the downwelling EICC forced by Ekman pumping over the BoB and remote forcing from the EIO (McCreary et al., 1993, 1996).

So the seasonal cycle of salinity in the western BoB (Fig. 9) suggests that the shallow equatorward EICC noted in December 1991 by Shetye et al. (1996) and the deep EICC noted in March–April 1991 by Shetye et al. (1993) are regular features. The HF radar and ADCP data reported here represent the first direct current measurement of the strong vertical shear during October–December in the EICC regime, but particularly so off Cuddalore (Fig. 10).

4. Spatial variation of the EICC

In the earlier section, we analysed the variability of the EICC at the ADCP locations. In this section, we begin by analysing the link between the EICC on the slope and shelf, followed by an analysis of the link between the currents observed at Gopalpur and Cuddalore. The section concludes by presenting the high-resolution spatial patterns seen in the radar data.

4.1. Cross-shelf variation

The EICC is a large-scale boundary current, but it is known to leave its imprint on the coastal sea level at seasonal (Shetye and Almeida, 1985; Shankar, 1998, 2000; Durand et al., 2008) and interannual (Clarke and Liu, 1994; Shankar, 1998; Srinivas et al., 2005; Aparna et al., 2012) time scales, implying a link between the EICC on the slope and shelf. Such a connection between the slope and shelf currents has

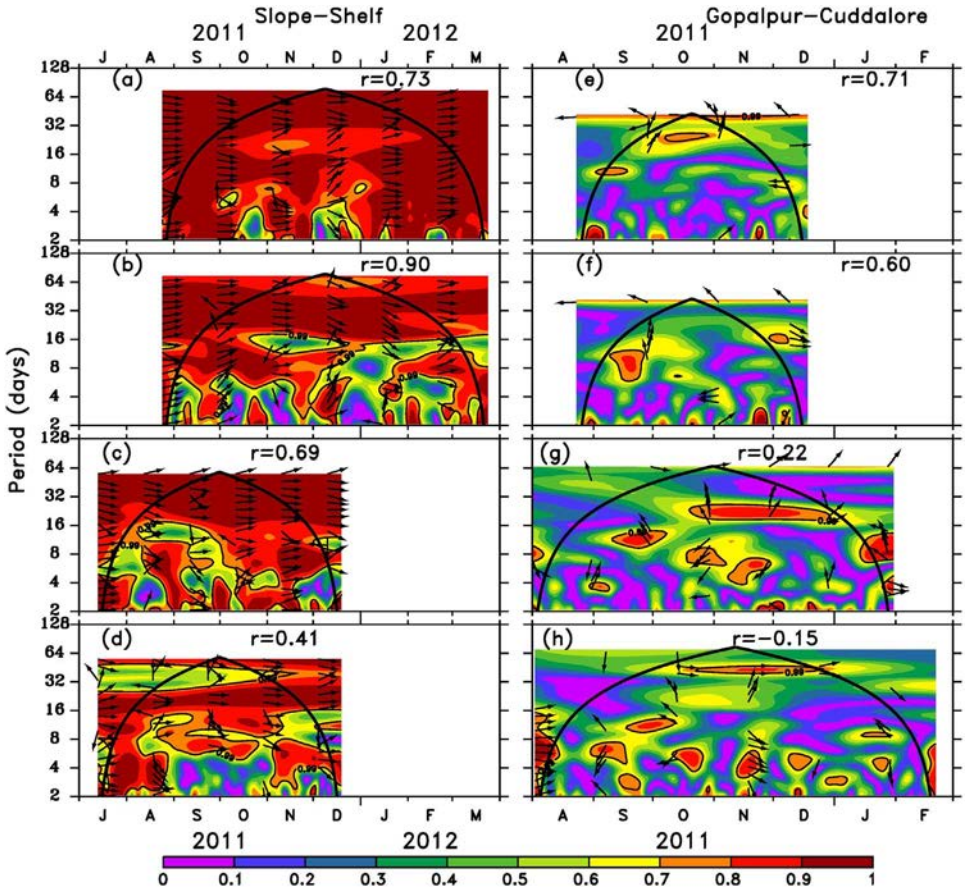

Fig. 11. Wavelet coherence between the slope and shelf (left panels) and between Gopalpur and Cuddalore (right panels). The wavelet coherence, unlike the correlation that is written in each panel, provides a measure of the correlation as a function of time and period. The thick black curve denotes the cone of influence and the coherence above the 99% significance level is marked by the black contour. (a) Correlation and coherence between the radar currents on the slope and shelf off Gopalpur. (b) As in (a), but for the ADCP currents at 40 m. (c) Correlation and coherence between the radar currents on the slope and shelf off Cuddalore. (d) As in (c), but for the ADCP currents at 40 m. (e) Correlation and coherence between the radar currents on the slope off Gopalpur and Cuddalore. (f) Correlation and coherence between the radar currents on the shelf off Gopalpur and Cuddalore. (g) Correlation and coherence between the 20 m ADCP currents on the shelf off Gopalpur and Cuddalore. (h) Correlation and coherence between the 40 m ADCP currents on the slope off Gopalpur and Cuddalore.

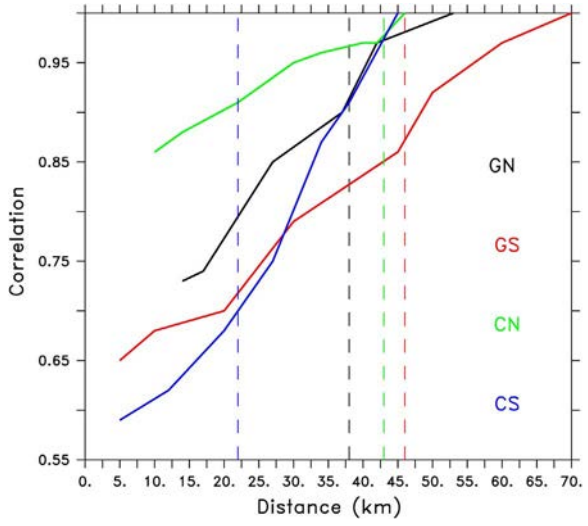

Fig. 12. Impact of the boundary current, the EICC, on the nearshore current based on the HF radar data. This figure shows the correlation between the slope current, roughly along the 1000 m isobath, and the current at radar data points on sections normal to the coast. The correlations are plotted for four sections, two each north and south of Gopalpur (GN and GS, respectively) and Cuddalore (CN and CS, respectively); these sections are marked in Fig. 1. The shelf break (200 m) is denoted by the vertical dashed lines. The abscissa represents the distance (km) from coast. The correlation at the outer edge of the section (rightmost point in each section) represents an auto-correlation (1) for the slope current.

already been shown for the much broader shelf off the Indian west coast (Amol et al., 2012, 2017; Amol, 2014).

The shelf in the western BoB is narrow (Fig. 1) and, as expected, we find a high correlation between the slope and shelf EICC at the surface (Fig. 11a) and at 40 m (Fig. 11b) off Gopalpur and at the surface off Cuddalore (Fig. 11c). The correlation and coherence at 40 m off Cuddalore are high and statistically significant (Fig. 11d), but lower than at the surface.

Since the shelf ADCP moorings are deployed at a depth of ~180 m (earlier ~100 m; Mukherjee et al., 2014), they are just ~10 km apart. Trawling on the shelf makes it difficult to deploy long-term moorings closer to the coast and such measurements are restricted to short durations (see Table 2 in (Mukherjee et al., 2014)). This dearth of nearshore current measurements underlies the importance of the HF radars. Though the spacing of the radars implies that the effect of GDOP (Chapman et al., 1997) rules out useful data over much of the alongshore radar range, data are available till close to the coast over a part of this radar domain. We pick data points along four transects, two each to the north and south of the ADCP moorings off Gopalpur and Cuddalore (Fig. 1) to check how the nearshore EICC correlates with the slope EICC. As shown in Fig. 12, the correlation at the location closest to the coast ranges between ~0.6–0.85 off Cuddalore; the correlations off Gopalpur are between ~0.65–0.72. All these correlations are significant at the 99% level and imply a strong imprint of the EICC on even the nearshore current.

4.2. Alongshore variation

Earlier studies have shown that the intraseasonal EICC decorrelates along the coast even on the continental slope (Durand et al., 2009; Mukherjee et al., 2014) and this decorrelation is evident in Fig. 11h. The alongshore correlation between the measurements at Gopalpur and Cuddalore confirms this lack of correlation at 20 m on the shelf (Fig. 11g) and at the surface on both slope (Fig. 11f) and shelf (Fig. 11e). This alongshore decorrelation at intraseasonal periods has been attributed to the presence of eddies (Durand et al., 2009; Mukherjee et al., 2014), which are seen in the altimeter data (Figs. 13,

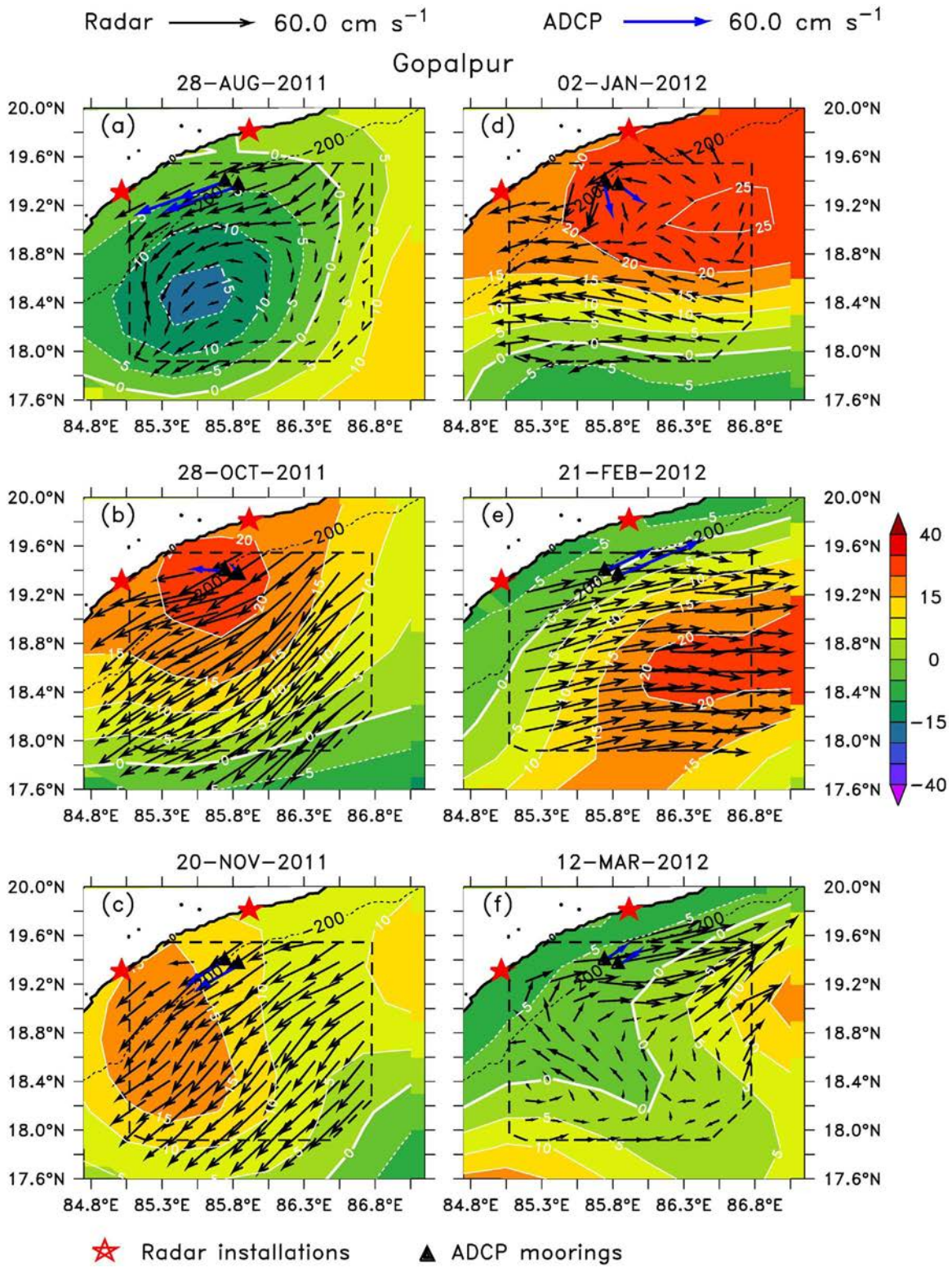

Fig. 13. Snapshots of sea-level anomalies (SLAs, cm) from the altimeter (contours) and 17-day-low-passed current vectors (cm s^{-1}) from the HF radar (black vectors) are shown for the region off Gopalpur. Contours are overlaid on the SLA. Also overlaid are the 17-day-low-passed ADCP current vectors (blue arrows). The 200 m isobath, denoting the shelf break, is shown by a dashed black curve.

14), and the downward bending of the beams associated with the coastal Kelvin waves (Nethery and Shankar, 2007). Amol et al. (2012) found high-energy cores at mid-depth on the shelf off the Indian west coast, implying a similar downward bending of beams associated with the shelf waves.

The wavelet coherence, which yields the correlation as a function of both time and periodicity, shows a better coherence on the shelf at both surface (Fig. 11e) and 20 m (Fig. 11g) in a band around ~22 days; a difference in phase is, however, evident between Gopalpur and Cuddalore. Likewise, the band around ~42 days is shows appreciable coherence at 40 m on the slope (Fig. 11h).

In summary, the alongshore correlation is patchy at the time scales

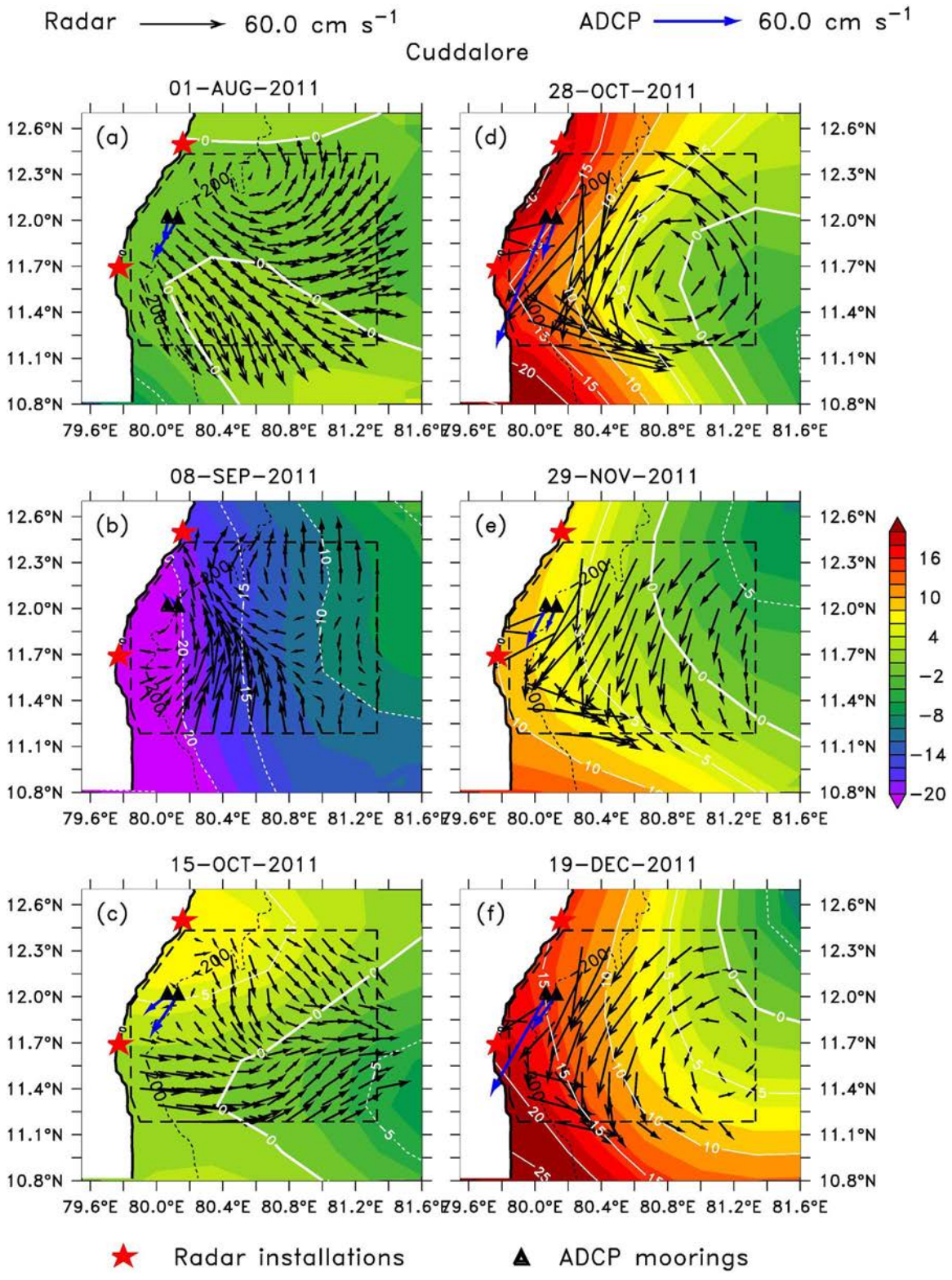

Fig. 14. Same as Fig. 13, but off Cuddalore.

resolved by the radar data.

4.3. Spatial patterns in the radar data

Altimeter SLAs and radar currents show mesoscale circulations associated with the EICC, but the spatial resolution of the HF radar, at ~6 km, is far superior to the 25 km resolution of the gridded altimeter data, and the circulation patterns seen in the radar data can therefore resolve finer scales than is possible with the altimeter (Figs. 13, 14). This difference in resolution is evident in the shorter scales in the radar currents associated with the cyclonic circulations seen off Cuddalore on 28 October and 19 December 2011 (Fig. 14).

If, however, one makes allowance for the coarser altimeter resolution, which can lead to spatial aliasing or a shift in the location of the

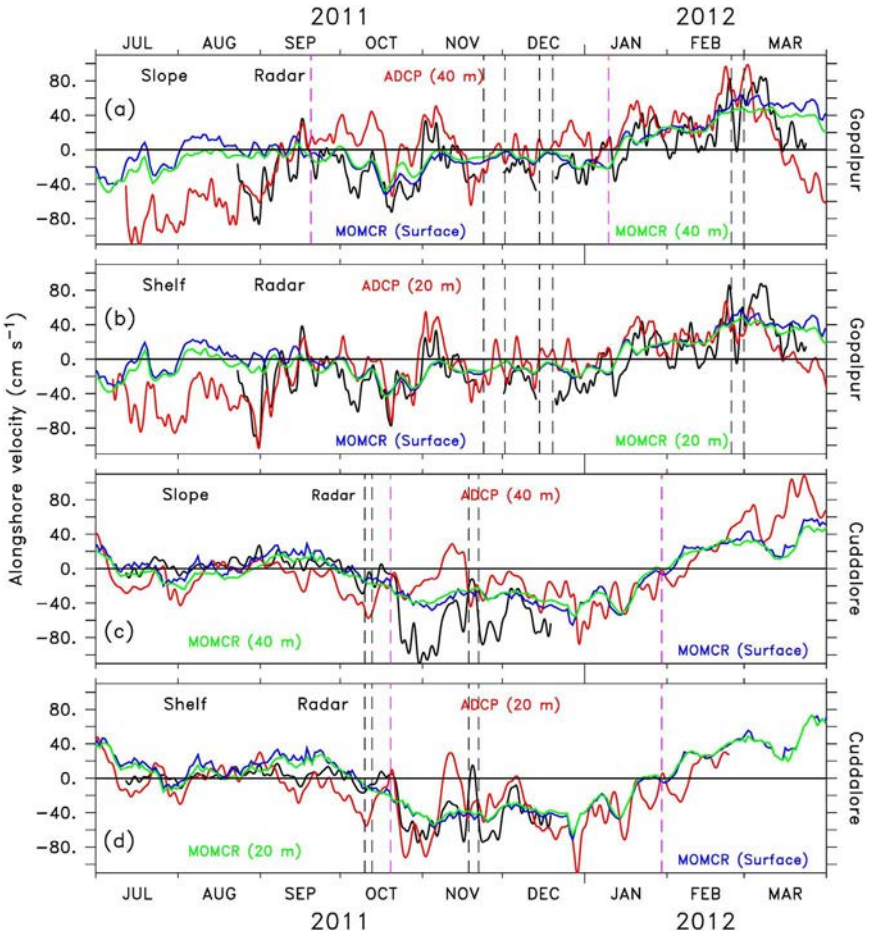

Fig. 15. Comparison of observed sub-inertial and simulated alongshore currents at the ADCP mooring locations on the slope and shelf off Gopalpur (top two panels) and Cuddalore (bottom two panels). The dashed vertical black pair of lines represent the bigger gaps in the radar data. The purple dashed vertical lines represent the period of the equatorward current flow at the station (see Fig. 10 for the period off Gopalpur and Cuddalore). (a) On the slope off Gopalpur. (b) On the shelf off Gopalpur. (c) On the slope off Cuddalore. (d) On the shelf off Cuddalore.

features not adequately resolved by the altimeter, then it is possible to discern a rough quasi-geostrophic balance between the surface currents and SLAs off both Gopalpur (Fig. 13d) and Cuddalore (Fig. 14f) on several occasions. Nevertheless, striking departures from this balance are also evident in the strong cross-shore flows off Gopalpur (Fig. 13e) and Cuddalore (Fig. 14b). On both these days, there is a strong Ekman flow offshore at the surface to match the low SLA at the coast (upwelling favourable). Note that the direction of the ADCP current on both days is as expected from geostrophy. Similarly, onshore flow is seen at both places to accompany downwelling on some days: an example is seen on 28-October at both locations (Fig. 13b, Fig. 14d), when the direction of the ADCP current is in accordance with geostrophy. Such cross-shore surface flow is not, however, seen on all days, with the data suggesting a quasi-geostrophic balance, particularly on the slope, between the alongshore EICC and the SLA field.

5. Discussion

5.1. Summary

We have presented the surface currents measured using HF radars off the indian east coast. This is the first description of HF radar data from the nio that go beyond presenting snapshots of the current. A key problem in using these data was the presence of data gaps of short durations. These gaps had precluded the use of standard time-series analysis tools like FFT and the wavelet transform. So the first step we took was to fill these gaps using an empirical method that is described in the Supplementary Material.

The radar data, filtered to remove the tides and the supra-inertial components, confirm several of the known features of the seasonal, surface EICC (Figs. 2, 3, 7, 8). The EICC flows equatorward during October–January in 2011 and poleward during January–March 2012. The radar current is sometimes in the same direction as the ADCP current at 40 m on the slope, but flows in the opposite direction at other times. The OSCAR current, which represents an average of the geostrophic and Ekman flow over the top 30 m (Bonjean and Lagerloef, 2002), generally follows the direction of the radar current, but its magnitude tends to average between the surface current measured by the radar and the ADCP current at 40 m. On the shelf, the radar current matches the ADCP current at 20 m, but not at 40 m, particularly off Cuddalore (Fig. 6).

So the HF radar data, used in conjunction with ADCP data, provide a measure of the shallowness of the surface current during some seasons. The combination of radar and ADCP data confirm what was seen in the hydrographic data (Shetye et al., 1991, 1993, 1996). The EICC is deep during February–March 2012, with the depth extending beyond 100 m on both shelf and slope. The poleward EICC during the summer monsoon of 2011 and the equatorward EICC during the winter monsoon (Shetye et al., 1996) of 2011 are shallower, with the ADCP current at 40 m often directed opposite to the surface current measured by the radar. The equatorward EICC during October–December shows a strong shear off Cuddalore and a weaker shear off Gopalpur (Fig. 10) that is due to a mixed layer that shallows to ~15–20 m (Fig. 9).

The radar data provide the first glimpse of high-frequency, intraseasonal variability of the surface EICC and the ADCP data of the sub-surface EICC. Intraseasonal variability off Gopalpur extends deeper and over the entire record compared to Cuddalore, where it tends to weaken with increasing depth and is restricted to the equatorward burst (Fig. 5).

The correlation between the shelf and slope EICC is high

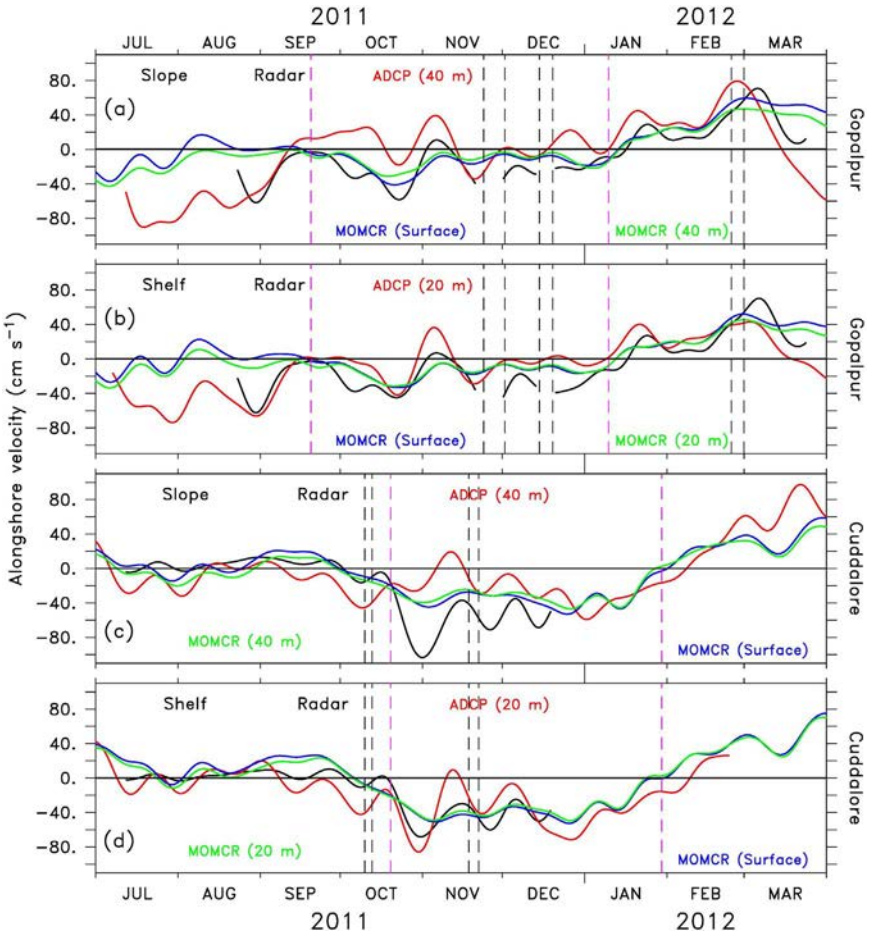

Fig. 16. Same as Fig. 15, but for the 17-day low-pass-filtered currents for both observations and simulation.

(Fig. 11a–d) owing to the narrow shelf off the Indian east coast. The shelf width (Fig. 1), ~50 km off Gopalpur and even less (~30 km) off Cuddalore, is less than the local Rossby radius of deformation (~60 km and ~80 km off Gopalpur and Cuddalore, respectively), implying a significant impact of the slope circulation on the shelf (Chapman and Brink, 1987). The high cross-correlation between the slope current and inner-shelf current at the surface (Fig. 12) shows the importance EICC dynamics even in the vicinity of the coast. Nearshore current measurements and model studies have shown that the large-scale boundary current leaves its mark on nearshore currents even on the Indian west coast, which has a broad shelf, at periods as short as ~4 days (Shetye et al., 2008; Shetye and Vijith, 2013; Amol et al., 2017) and the radar data presented here provide confirmation using reliable direct measurements of the nearshore current. In addition, mesoscale features are also prominent off Gopalpur and they leave a mark on the EICC (Fig. 13 and Animation S1 in the Supplementary Material).

The significance of the HF radar data is threefold. First, unlike the subsurface ADCP moorings, these data are available in near-real-time. Hence, they can be used to validate forecasts currently being made by INCOIS and for applications that require such real-time data on surface currents. An example is tracking oil spills and predicting their trajectory. Second, the radar provides an estimate of the surface current at a spatial and temporal resolution not possible with other instruments. The HF radar provides a way to map changes in the flow at short temporal and small spatial scales. Examples of such short bursts are seen during September and November 2011 off Gopalpur (Figs. 2, 7). The spatial and temporal resolution of the radar data implies that one useful application is in the advisories for potential fishery zones (PFZs; Solanki et al., 2010). Observations show that the fronts and filaments associated with such PFZs are advected by the mean current (Vipin et al., 2015). An example of the potential of these data is animated in maps of sea surface temperature and radar currents (Supplementary Material; Animation S2). Third, the radar data presented here provide for the first time a measure of the nearshore current relative to the EICC, which is essentially a boundary current. Such direct current measurements are necessary in order to interpret the high-frequency changes seen in, for example, the biogeochemistry (see Figs. 2–4 in Maya et al., 2011) or the barnacle life cycle (see Fig. 5 in Gaonkar et al., 2012) in the nearshore waters off the Indian coast.

5.2. OGCM simulation of the EICC

Mukherjee et al. (2017) show that a state-of-the-art OGCM with a resolution of 0.1° × 0.1° is able to simulate well only the seasonal cycle of the EICC; the model performance is not as good at intraseasonal periods. They also show that there exists a difference between the model current at 40 m, of which the ADCP data provide a measure, and the surface, for which they had no data. A comparison of the model currents with the sub-inertial (Fig. 15a,c) or the 17-day low-passed current (Fig. 16a,c) shows that the model currents on the slope at the surface and 40 m are not as different as in the observations. There is not much difference between the model current on the slope and the shelf (Fig. 15b,d, Fig. 16b,d) too. As one would expect, the performance of the model degrades with decreasing period (Fig. 17).

In particular, the model current does not reverse with depth as often as the observed current does (Fig. 16) and the model also produces weaker upward phase propagation (figure not shown). Hence, though there does exist a vertical shear in the model, in which the surface salinity is relaxed to climatology, it is much weaker than the observed vertical shear (Fig. 10).

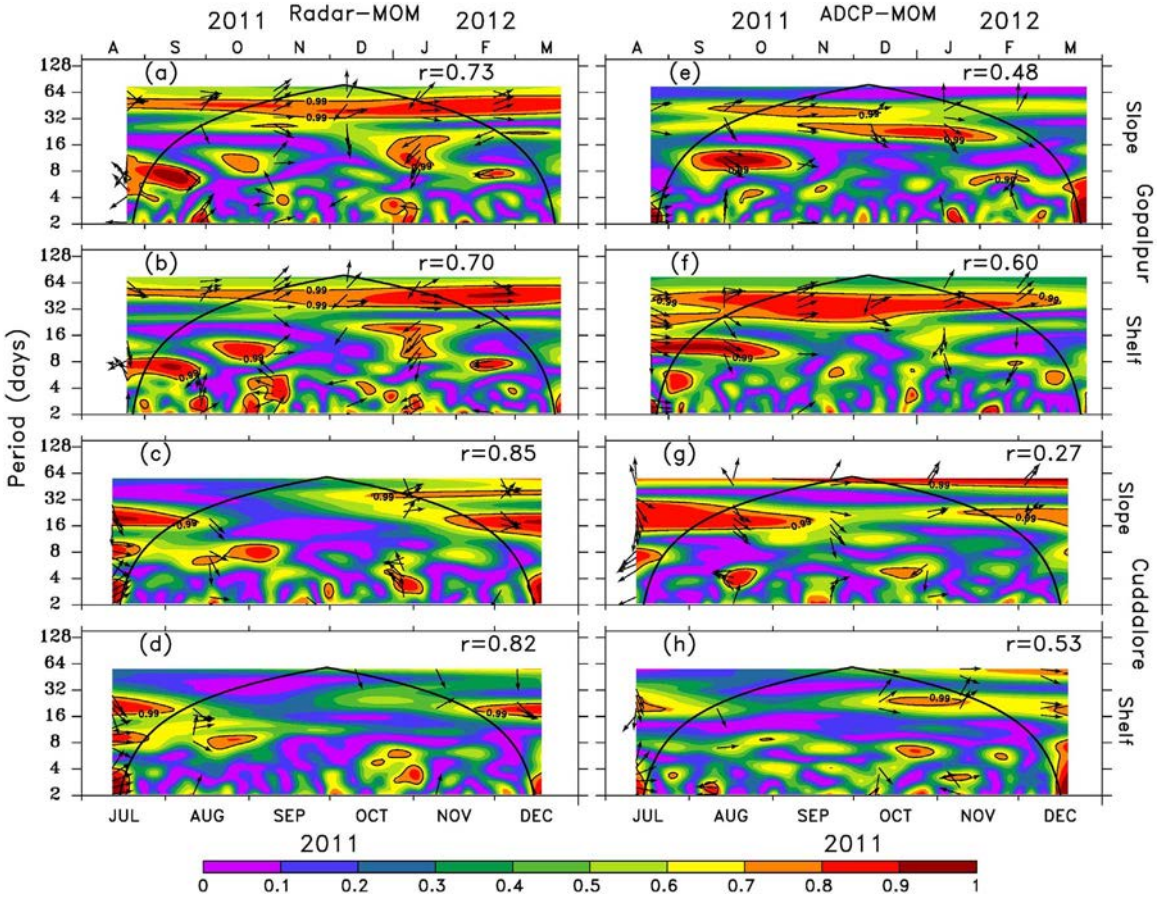

Fig. 17. Wavelet coherence between observed and simulated alongshore currents at the ADCP mooring locations on the shelf and slope. The wavelet coherence, unlike the correlation that is written in each panel, provides a measure of the correlation as a function of time and period. The thick black curve denotes the cone of influence and the coherence above the 99% significance level is marked by the black contour. (a) Correlation and coherence between the radar and simulated currents on the shelf off Gopalpur. (b) As in (a), but for the slope. (c) Correlation and coherence between the radar and simulated currents on the shelf off Cuddalore. (d) As in (c), but for the slope. (e) Correlation and coherence between the ADCP (20 m) and simulated currents on the shelf off Gopalpur. (f) Correlation and coherence between the ADCP (40 m) currents on the slope off Gopalpur. (g) As in (e), but for Cuddalore. (h) As in (f), but for Cuddalore.

6. Conclusions

The HF radar data provide a measure of the surface current, which was not available from the ADCP data presented earlier for the Indian west (Amol et al., 2014) and east (Mukherjee et al., 2014) coasts. When used in conjunction with the ADCP data, the radar data permit an analysis of the current over the water column on the continental shelf. This combination of instruments confirms that the EICC flows poleward as a deep current during February–March and a shallow current during October-November. During the summer monsoon, when the EICC flows poleward, and October–December, when the EICC flows equatorward, the current is shallow (<40 m deep), except towards the northern end of the coast. This seasonal cycle of the EICC is depicted in the schematic in Fig. 18.

These direct current measurements do much more, however, than merely confirm what was known over two decades ago. They show, for example, that the EICC flows equatorward at the surface throughout the winter monsoon, but is not a shallow current over the entire season (Figs. 2, 3, 7, 8): poleward and equatorward bursts are evident below this surface layer, implying that the equatorward current is shallow for some time, then deepens to ~100 m or more before shallowing again. Thus, both poleward and equatorward flows show variability at periods of the order of 20–45 days, implying that the EICC direction is the same over the top ~100 m for short durations. In almost all these events, one sees upward phase propagation, a sign of propagating Kelvin or shelf waves. The radar data show that the upward propagation of phase evident in the ADCP data does not always extend to the surface.

The nearshore imprint of the boundary current has an important implication for environmental impact assessments (EIAs). As India industrialises and trade increases, the number of industrial projects in the coastal zone is increasing. The EIA studies for such projects typically use small-domain model simulations, assuming that the nearshore current of interest is dominated by local processes. The data presented in this paper, along with data from the Indian west coast and model studies cited above, prove the limitation of such limited-domain model studies. Just as the connectivity of the basin makes it necessary to model the entire Indian Ocean to simulate even the seasonal cycle of the boundary current or coastal sea level anywhere off the Indian coast (McCreary et al., 1993; Shankar et al., 2002), the nearshore signature of the large-scale EICC, which is forced in part by remote winds, necessitates modelling a large fraction of the Indian coastal regime to simulate the current or sea level in any part. Since the EIAs require an accurate simulation of the near-coastal current, this large domain must be modelled at a high enough resolution, a task that is likely to demand a set of nested model domains. In order to enable validation of such modelling studies, it is important to extend the promising HF radar network to cover the entire Indian coast, as has been done in the United States (http://cordc.ucsd.edu/projects/mapping/maps/).

Acknowledgments

We thank Dr. B. K. Jena of NIOT and the INCOIS data centre for the HF radar data and Dr. M. Atmanand, Dr. S. S. C. Shenoi, and Dr. S. Nayak for making the data available. Funding for this work was made

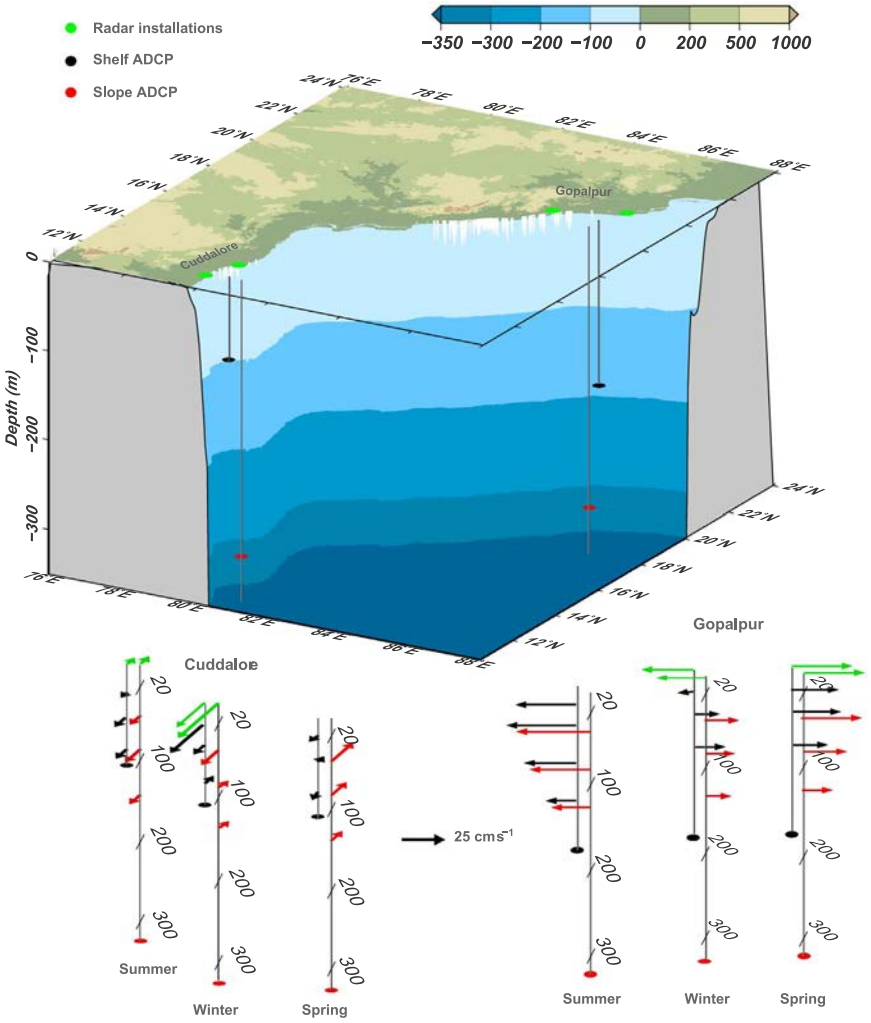

Fig. 18. Schematic showing the vertical profile of the alongshore EICC at the ADCP locations on the shelf and slope off Gopalpur and Cuddalore. The colour key represents the bathymetry of the ocean as well as the land topography. The shelf ADCP at Gopalpur (Cuddalore) was deployed at ~100 m (~180 m); the shelf ADCP was deployed just above the anchor weight and the acoustic releases. At both locations, the slope ADCP was deployed at ~350 m in a water-column depth of ~1100 m; hence, the slope mooring line extends below the depth at which the ADCP float is shown in the figure. Green arrows are used to represent the HF radar current and black (red) arrows for the ADCP current on the continental shelf (slope). The vertical profiles are plotted for the currents averaged over 12-July-2011 to 31-August-2011 for the summer monsoon, 1-October-2011 to 15-November-2011 for the winter monsoon, and 20-January-2012 to 20-March-2012 for spring; these periods are denoted by the light grey highlighting in Figs. 2, 3, 7, 8. The HF radar data, which are used to denote the surface current, are not available during the summer monsoon of 2011 at Gopalpur and during spring 2012 at Cuddalore. The vectors are drawn to match the coastline orientation in the map. At Gopalpur, the coastline is roughly "horizontal" and the arrow pointing to the right (left) represents a poleward (equatorward) current. At Cuddalore, the coastline orientation is roughly at 45° to the horizontal axis and the arrow pointing to the right (left) represents poleward (equatorward) flow.

available by the Council of Scientific and Industrial Research (CSIR) under its OCEAN FINDER programme and the Ministry of Earth Sciences (MoES, via INCOIS) under its Ocean Observing Systems programme. We acknowledge two anonymous reviewers for their critical comments, which helped improve the manuscript considerably. The FORTRAN code for wavelet analysis and the *R* package for wavelet coherence spectra were downloaded from http://paos.colorado.edu/research/wavelets and http://tocsy.agnld.uni-potsdam.de/wavelets, respectively. SM acknowledges funding from CSIR under its research-fellowship programme. The wavelet software was downloaded from http://paos.colorado.edu/. Ferret was used for analysis and Ferret and Generic Mapping Tools (GMT) for graphics; SM acknowledges P. Amol for useful discussions, Vineet Jain and Charls Antony for helping him with GMT, and Anil Kumar for helping him with the schematic, and also Vineet Jain, V. Vijith and Remya R. for their suggestion on the same. We acknowledge C. Gokul for helping with HF radar data. This is CSIR-NIO contribution 8764 and INCOIS contribution 305.

Appendix A. Supplementary data

Supplementary data associated with this article can be found in the online version at http://dx.doi.org/10.1016/j.csr.2017.08.020.

References

Amol, P., 2014. Intraseasonal Variability of Currents Along West Coast of India (Ph.D. thesis). Goa University, Goa, India.

Amol, P., Fernando, V., Vijith, V., Pednekar, P., Singh, J., 2017. Influence of west-coast winds on the shelf circulation off the central west coast of India. Unpublished X, X-Y. Personal communication.

Amol, P., Shankar, D., Aparna, S.G., Shenoi, S.S.C., Fernando, V., Shetye, S.R., Mukherjee, A., Agarvadekar, Y., Khalap, S.T., Satelkar, N.P., 2012. Observational evidence from direct current measurements for propagation of remotely forced waves on the shelf off the west coast of India. J. Geophys. Res. 117. http://dx.doi.org/10.1029/2011JC007606.

Amol, P., Shankar, D., Fernando, V., Mukherjee, A., Aparna, S.G., Fernandes, R., Michael, G.S., Khalap, S.T., Satelkar, N.P., Agarvadekar, Y., Gaonkar, M.G., Tari, A.P., Kankonkar, A., Vernekar, S.P., 2014. Observed intraseasonal and seasonal variability of the West India Coastal Current on the continental slope. J. Earth Syst. Sci. 123, 1045–1074. http://dx.doi.org/10.1007/s12040-014-0449-5.

Aparna, S.G., McCreary, J.P., Shankar, D., Vinayachandran, P.N., 2012. Signatures of the Indian Ocean Dipole and El Nino-Southern Oscillation events in sea level variations in the Bay of Bengal. J. Geophys. Res. 117, C10012. http://dx.doi.org/10.1029/2012JC008055.

AVISO, 1996. AVISO User Handbook: Merged TOPEX/Poseidon Products. Technical Report. Collecte Localisation Satellites. France.

Bell, C., Vassie, J.M., Woodworth, P.L., 1998. POL/PSMSL Tidal Analysis733 Software Kit 2000 (TASK-2000). Permanent Service for734 Mean Sea Level, UK Technical Report.

Bonjean, F., Lagerloef, G.S.E., 2002. Diagnostic model and analysis of the surface currents in the tropical Pacific Ocean. J. Phys. Oceanogr. 32, 2938–2954. http://dx.doi.org/10.1175/1520-0485(2002)032<2938:DMAAOT>2.0.CO;2.

Chapman, D.C., Brink, K.H., 1987. Shelf and slope circulation induced by fluctuating offshore forcing. J. Geophys. Res. 92, 11741–11759. http://dx.doi.org/10.1029/JC092iC11p11741.

Chapman, R.D., Shay, L.K., Graber, H.C., Edson, J.B., Karachintsev, A., Trump, C.L., Ross, D.B., 1997. On the accuracy of hf radar surface current measurements: intercomparisons with ship-based sensors. J. Geophys. Res. 102, 737–748. http://dx.doi.org/10.1029/97JC00049.

Chatterjee, A., Shankar, D., McCreary, J.P., Vinayachandran, P.N., 2013. Yanai waves in the western equatorial Indian Ocean. J. Geophys. Res. 118, 1556–1570. http://dx.doi.org/10.1002/jgrc.20121.

Chatterjee, A., Shankar, D., McCreary, J.P., Vinayachandran, P.N., Mukherjee, A., 2017. Dynamics of Andaman sea circulation and its role in connecting the equatorial Indian Ocean to the Bay of Bengal. J. Geophys. Res. 122. http://dx.doi.org/10.1002/2016JC012300.

Chatterjee, A., Shankar, D., Shenoi, S.S.C., Reddy, G.V., Michael, G.S., Ravichandran, M.,

Gopalkrishna, V.V., Rao, E.P.R., Bhaskar, T.V.S.U., Sanjeevan, V.N., 2012. A new atlas of temperature and salinity for the north Indian Ocean. J. Earth Syst. Sci. 121, 559–593. http://dx.doi.org/10.1007/s12040-012-0191-9.

Chen, G., Wang, D., Hou, Y., 2012. The features and interannual variability mechanism of mesoscale eddies in the Bay of Bengal. Cont. Shelf Res. 47, 178–185. http://dx.doi.org/10.1016/j.csr.2012.07.011.

Cheng, X., Xie, S.P., McCreary, J.P., Qi, Y., Du, Y., 2013. Intraseasonal variability of sea surface height in the Bay of Bengal. J. Geophys. Res. 118, 816–830. http://dx.doi.org/10.1002/jgrc.20075.

Clarke, A.J., Liu, X., 1994. Interannual sea level in the northern and eastern Indian Ocean. J. Phys. Oceanogr. 24, 1224–1235. http://dx.doi.org/10.1175/1520-0485(1994)0242.0.CO;2.

Cosoli, S., Mazzoldi, A., Gačic, M., 2010. Validation of surface current measurements in the northern Adriatic Sea from high-frequency radars. J. Atmos. Ocean. Technol. 27, 908–919. http://dx.doi.org/10.1175/2009JTECHO680.1.

Cutler, A.N., 1984. Surface Currents of the Indian Ocean (to25∘S, 100∘771 E): Compiled from Historical Data Archived by the Meteorological Office, Bracknell, UK. Metorological Office, UK Technical Report.

Durand, F., Shankar, D., Birol, F., Shenoi, S., 2009. Spatiotemporal structure of the East India Coastal Current from satellite altimetry. J. Geophys. Res. 114. http://dx.doi.org/10.1029/2008JC004807.

Durand, F., Shankar, D., Birol, F., Shenoi, S.S.C., 2008. Estimating boundary currents from satellite altimetry: a case study for the east coast of India. J. Oceanogr. 64, 831–845.

Durand, F., Shankar, D., Montegut, C.D., Shenoi, S.S.C., Blanke, B., Madec, G., 2007. Modeling the barrier-layer formation in the southeastern Arabian Sea. J. Clim. 20, 2109–2120. http://dx.doi.org/10.1175/JCLI4112.1.

Eigenheer, A., Quadfasel, D., 2000. Seasonal variability of the Bay of Bengal circulation inferred from TOPEX/Poseidon altimetry. J. Geophys. Res. 105, 3243–3252. http://dx.doi.org/10.1029/1999JC900291.

Emery, B., Washburn, L., Harlan, J., 2004. Evaluating radial current measurements from CODAR high-frequency radars with moored current meters. J. Atmos. Ocean. Technol. 21, 1259–1271. http://dx.doi.org/10.1175/1520-0426(2004)021<1259:ERCMFC>2.0.CO;2.

Gaonkar, C., Samiksha, S.V., George, G., Aboobacker, V.M., Vethamony, P., Anil, A.C., 2012. Numerical simulations of barnacle larval dispersion coupled with field observations on larval abundance, settlement and recruitment in a tropical monsoon influenced coastal marine environment. J. Mar. Syst. 94, 218–234. http://dx.doi.org/10.1016/j.jmarsys.2011.12.

Griffies, S.M., 2009. Elements of MOM4p1. Technical Report. Available online at 〈http://www.gfdl.noaa.gov〉.

Han, W., McCreary, J.P., Kohler, K.E., 2001. Influence of precipitation minus evaporation and Bay of Bengal rivers on dynamics, thermodynamics, and mixed layer physics in the upper Indian Ocean. J. Geophys. Res. 106, 6895–6916. http://dx.doi.org/10.1029/2000JC000403.

John, M., Jena, B.K., Sivakholundu, K.M., 2015. Surface current and wave measurement during cyclone Phailin by high-frequency radars along the Indian coast. Curr. Sci. 108, 405.

Kalnay, E., kanamitsu, M., Kistler, R., Collins, W., Deaven, D., Gandin, L., Iredell, M., Saha, S., White, G., Woollen, J., Zhu, Y., Chelliah, M., Ebisuzaki, W., Higgins, W., Janowiak, J., Mo, K.C., Ropelewski, C., Wang, J., Leetmaa, A., Reynolds, R., Jenne, R., Joseph, D., 1996. The NCAP/NCAR 40-year Reanalysis project. Bull. Am. Meteorol. Soc. 77 (3), 437–471. http://dx.doi.org/10.1175/1520-0477(1996)077 2.0.CO;2.

Kuang, L., Blumberg, A.F., Georgas, N., 2012. Assessing the fidelity of surface currents from a coastal ocean model and HF radar using drifting buoys in the Middle Atlantic Bight. Ocean Dyn. 62, 1229–1243. http://dx.doi.org/10.1007/s10236-012-0556-2.

Kurian, J., Vinayachandran, P.N., 2007. Mechanisms of formation of Arabian Sea mini warm pool in a high-resolution OGCM. J. Geophys. Res. 112, C05009. http://dx.doi.org/10.1029/2006JC003631.

Kurien, P., Ikeda, M., Valsala, V.K., 2010. Mesoscale variability along the east coast of India in spring as revealed from satellite data and OGCM simulations. J. Oceanogr. 66, 273–289. http://dx.doi.org/10.1007/s10872-010-0024-x.

Kutsuwada, K., McPhaden, M., 2002. Intraseasonal variations in the upper equatorial Pacific Ocean prior to and during the 1997-98 El Niño. J. Phys. Oceanogr. 32, 1133–1149. http://dx.doi.org/10.1175/1520-0485(2002)032<1133:IVITUE>2.0.CO;2.

Legeckis, R., 1987. Satellite observations of a western boundary current in the Bay of Bengal. J. Geophys. Res. 92, 12974–12978. http://dx.doi.org/10.1029/JC092iC12p12974.

Lukas, R.B., Lindström, E.J., 1991. The mixed layer of the western equatorial Pacific Ocean. J. Geophys. Res. 96, 3343–3357. http://dx.doi.org/10.1029/90JC01951.

Mariano, A.J., Ryan, E.H., Perkins, B.D., Smithers, S., 1995. The Mariano829 Global Surface Velocity Analysis 1.0. USCG Report CG-D-34-95. Office830 of Engineering, Logistics, and Development, U.S. Coast Guard.

Maya, M.V., Karapurkar, S.G., Naik, H., Roy, R., Shenoy, D.M., Naqvi, S.W.A., 2011. Intra-annual variability of carbon and nitrogen stable isotopes in suspended organic matter in waters of the western continental shelf of India. Biogeosciences 8, 3441–3456. http://dx.doi.org/10.5194/bg-8-3441-2011.

McCreary, J.P., Han, W., Shankar, D., Shetye, S.R., 1996. Dynamics of the East India Coastal Current 2. Numerical solutions. J. Geophys. Res. 101, 13993–14010. http://dx.doi.org/10.1029/96JC00560.

McCreary, J.P., Kundu, P.K., Molinari, R.L., 1993. A numerical investigation of dynamics, thermodynamics and mixed-layer processes in the Indian Ocean. Progress. Oceanogr. 31, 181–244. http://dx.doi.org/10.1016/0079-6611(93)90002-U.

Mukherjee, A., Shankar, D., Aparna, S.G., Amol, P., Fernando, V., Fernandes, R., Khalap, S.T., Narayan, S., Agarvadekar, Y., Gaonkar, M.G., Tari, A.P., Kankonkar, A., Vernekar, S.P., 2013. Near-inertial currents off the east coast of India. Cont. Shelf Res. 55, 29–39. http://dx.doi.org/10.1016/j.csr.2013.01.007.

Mukherjee, A., Shankar, D., Chatterjee, A., Vinayachandran, P.N., 2017. Numerical simulation of the observed near-surface East India Coastal Current on the continental slope. Climate Dynamics. http://dx.doi.org/10.1007/s00382-017-3856-x.

Mukherjee, A., Shankar, D., Fernando, V., Amol, P., Aparna, S.G., Fernandes, R., Michael, G.S., Khalap, S.T., Satelkar, N.P., Agarvadekar, Y., Gaonkar, M.G., Tari, A.P., Kankonkar, A., Vernekar, S.P., 2014. Observed seasonal and intraseasonal variability of the East India Coastal Current on the continental slope. J. Earth Syst. Sci. 123, 1197–1232. http://dx.doi.org/10.1007/s12040-014-0471-7.

Nethery, D., Shankar, D., 2007. Vertical propagation of baroclinic Kelvin waves along the west coast of India. J. Earth Syst. Sci. 116, 331–339. http://dx.doi.org/10.1007/s12040-007-0030-6.

Ohlmann, C., White, P., Washburn, L., Emery, B., Terrill, E., Otero, M., 2007. Interpretation of coastal HF radar-derived surface currents with high-resolution drifter data. J. Atmos. Ocean. Technol. 24, 666–680. http://dx.doi.org/10.1175/JTECH1998.1.

Paduan, J.D., Washburn, L., 2013. High-frequency radar observations of ocean surface currents. Annu. Rev. Mar. Sci. 5, 115–136. http://dx.doi.org/10.1146/annurev-marine-121211-172315.

Robinson, A.M., Wyatt, L.R., Howarth, M.J., 2011. A two-year comparison between HF radar and ADCP current measurements in Liverpool Bay. J. Oper. Oceanogr. 4, 33–45. http://dx.doi.org/10.1080/1755876X.2011.11020121.

Röhrs, J., Sperrevik, A.K., Christensen, K.H., Broström, G., Breivik, Ø., 2015. Comparison of HF radar measurements with Eulerian and Lagrangian surface currents. Ocean Dyn. 65, 679–690. http://dx.doi.org/10.1007/s10236-015-0828-8.

Schott, F.A., McCreary, J.P., 2001. The monsoon circulation of the Indian Ocean. Prog. Oceanogr. 51, 1–123. http://dx.doi.org/10.1016/S0079-6611(01)00083-0.

Shankar, D., 1998. Low-frequency variability of sea level along the coast of879 India (Ph.D. thesis). Goa University, Goa, India.

Shankar, D., 2000. Seasonal cycle of sea level and currents along the coast of India. Curr. Sci. 78, 279–288.

Shankar, D., McCreary, J.P., Han, W., Shetye, S.R., 1996. Dynamics of the East India Coastal Current 1. Analytic solutions forced by interior Ekman pumping and local alongshore winds. J. Geophys. Res. 101, 13975–13991. http://dx.doi.org/10.1029/96JC00559.

Shankar, D., Vinayachandran, P.N., Unnikrishnan, A.S., 2002. The monsoon currents in the north Indian Ocean. Prog. Oceanogr. 52, 63–120. http://dx.doi.org/10.1016/S0079-6611(02)00024-1.

Shetye, S., Shenoi, S., Gouveia, A., Michael, G., Sundar, D., Nampoothiri, G., 1991. Wind-driven coastal upwelling along the western boundary of the Bay of Bengal during the southwest monsoon. Cont. Shelf Res. 11, 1397–1408. http://dx.doi.org/10.1016/0278-4343(91)90042-5.

Shetye, S.R., Almeida, A.M., 1985. An examination of the factors that influence the monthly-mean sea level along the coast of India. In: IOC/Unesco Workshop on Regional Co-operation in Marine Science in the Central Indian Ocean and Adjacent Seas and Gulfs, Colombo, Sri Lanka; pp. 87–104.

Shetye, S.R., Gouveia, A.D., 1998. Coastal circulation in the north Indian Ocean: coastal segment (14, SW). Sea 11, 523–556.

Shetye, S.R., Gouveia, A.D., Shankar, D., Shenoi, S.S.C., Vinayachandran, P.N., Sundar, D., Michael, G.S., Nampoothiri, G., 1996. Hydrography and circulation in the western Bay of Bengal during the northeast monsoon. J. Geophys. Res. 101, 14011–14025. http://dx.doi.org/10.1029/95JC03307.

Shetye, S.R., Gouveia, A.D., Shenoi, S.S.C., Sundar, D., Michael, G.S., Nampoothiri, G., 1993. The western boundary current of the seasonal subtropical gyre in the Bay of Bengal. J. Geophys. Res. 98, 945–954. http://dx.doi.org/10.1029/92JC02070.

Shetye, S.R., Suresh, I., Shankar, D., Sundar, D., Jayakumar, S., Mehra, P., Prabhudesai, R.G., Pednekar, P.S., 2008. Observational evidence for remote forcing of the West India Coastal Current. J. Geophys. Res. 113. http://dx.doi.org/10.1029/2008JC004874.

Shetye, S.R., Vijith, V., 2013. Sub-tidal water-level oscillations in the Mandovi estuary, west coast of India. Estuar. Coast. Shelf Sci. 134, 1–10. http://dx.doi.org/10.1016/j.ecss.2013.09.016.

Sindhu, B., Suresh, I., Unnikrishnan, A., Bhatkar, N., Neetu, S., Michael, G., 2007. Improved bathymetric datasets for the shallow water regions in the Indian Ocean. J. Earth Syst. Sci. 116, 261–274. http://dx.doi.org/10.1007/s12040-007-0025-3.

Solanki, H.U., Prakash, P., Dwivedi, R.M., Nayak, S.R., Kulkarni, A., Somvamshi, V.S., 2010. Synergistic application of oceanographic variables from multi-satellite sensors for forecasting potential fishing zones: methodology and validation results. Int. J. Remote Sens. 31, 775–789. http://dx.doi.org/10.1080/01431160902897833.

Srinivas, K., Kumar, P.K.D., Revichandran, C., 2005. ENSO signature in the sea level along the coastline of the Indian subcontinent. Indian J. Mar. Sci. 34, 225–236.

Vialard, J., Delecluse, P., 1998. An OGCM study for the TOGA decade. Part II: barrier-layer formation and variability. J. Phys. Oceanogr. 28, 1089–1106. http://dx.doi.org/10.1175/1520-0485(1998)028 2.0.CO;2.

Vialard, J., Shenoi, S.S.C., McCreary, J.P., Shankar, D., Durand, F., Fernando, V., Shetye, S.R., 2009. Intraseasonal response of the northern Indian Ocean coastal waveguide to the Madden-Julian oscillation. Geophys. Res. Lett. 36. http://dx.doi.org/10.1029/2009GL038450.

Vinayachandran, P.N., Shetye, S.R., Sengupta, D., Gadgil, S., 1996. Forcing mechanisms of the Bay of Bengal circulation. Curr. Sci. 71, 753–763.

Vipin, P., Sarkar, K., Aparna, S.G., Shankar, D., Sarma, V.V.S.S., Gracias, D.G., Krishna, M.S., Srikanth, G., Mandal, R., Rao, E.P.R., Rao, N.S., 2015. Evolution and sub-surface characteristics of a sea-surface temperature filament and front in the north-eastern Arabian Sea during November-December 2012. J. Mar. Syst. 150, 1–11. http://dx.doi.org/10.1016/j.jmarsys.2015.05.003.